NASA Technical Memorandum 81239

Simulation Study of the Interaction Between the Propulsion and Flight Control Systems of a Subsonic Lift Fan VTOL

Bruce E. Tinling and Gary L. Cole

November 1980

National Aeronautics and
Space Administration

NASA Technical Memorandum 81239

Simulation Study of the Interaction Between the Propulsion and Flight Control Systems of a Subsonic Lift Fan VTOL

Bruce E. Tinling, Ames Research Center, Moffett Field, California
Gary L. Cole, Lewis Research Center, Cleveland, Ohio

National Aeronautics and
Space Administration

Ames Research Center
Moffett Field, California 94035

NOTATION

Airframe and Control System Variables

$\dot{h}$	vertical velocity of airplane center of gravity
$\dot{h}_c$	vertical velocity command from autopilot
$\ddot{h}$	vertical acceleration of airplane center of gravity
GW	gross weight
I_x, I_y, I_z	airplane moments of inertia about body axes
I_{xz}	airplane product of inertia with respect to x and z body axes
s	Laplace transform variable
V	airspeed
V_x	airplane longitudinal inertial velocity
$\dot{V}_x$	airplane longitudinal inertial acceleration
$\dot{V}_{x_c}$	airplane longitudinal acceleration command from autopilot
y	localizer error
α	airplane angle of attack
β	airplane angle of sideslip
δ_{AI}	control system input to ailerons
δ_{HI}	control system input to elevator
$\delta_{\dot{h}}$	pilot control input to vertical controller
$\delta_{I_\phi}, \delta_{I_\theta}, \delta_{I_\psi}$	pilot control inputs to attitude control system
δ_{RI}	control system input to rudder
$\delta_{t_f}, \delta_{t_\beta}$	control system inputs to power lever system
δ_{v_f}	power lever system input to fuel control
δ_{v_β}	power lever system input to blade control
$\delta_{\dot{v}_x}$	pilot control input to horizontal acceleration controller
δ_ϕ	roll control system input to blade control

δ_θ	pitch control system input to blade control
δ_ψ	yaw control system input to louver control
$\hat{\delta}_\phi$	feedback quantity for roll controller derived from blade actuator position
$\hat{\delta}_\theta$	feedback quantity for pitch controller derived from blade actuator position
$\hat{\delta}_{t_\beta}$	feedback quantity for height controller derived from blade actuator position
Δh	altitude error
ϕ	roll angle
$\dot{\phi}$	first time derivative of ϕ
$\ddot{\phi}$	second time derivative of ϕ
ϕ_c	roll angle commanded by autopilot
θ	pitch angle
$\dot{\theta}$	first time derivative of θ
$\ddot{\theta}$	second time derivative of θ
θ_c	pitch angle commanded by autopilot
θ_j	thrust vector angle (90° normal to body x axis)
ζ_{TL}	thrust vector command input to louvers

Propulsion System Parameters

General form: ABC x_1x_2y, where ABC refers to the physical quantity, x_1 and x_2 refer to the location within the engine, and y refers to the engine number (see figs. 1 and 2).

ALT	altitude
BETAF	fan blade angle
BETN	command to fan blade actuator
DB	fan blade actuator deadband
DTT	ambient atmospheric temperature

FG	net thrust
FGROS	gross thrust
HPF	power absorbed by fan
HP1T	engine power available to fans
HP2T	engine power available to compressor
HP2C	power absorbed by compressor
I_{HP}, I_{LP}	moments of inertia of high- and low-pressure engine rotors
MNO	Mach number at inlet
NH	engine angular velocity
NL	fan angular velocity
PCNHD	engine corrected speed command, percent
PCNHR	engine corrected speed, percent
PS	static pressure
PT	total pressure
SM	fan stall margin
TT	total temperatures
V	flow velocities
W	engine main flows
WA	duct mass flows
WFH	fuel mass flow rate
WG	mass flow of combined fan and engine nozzles
XNPCT	fan mechanical speed, percent
τ_n	time constant in heat-soak transfer function

SIMULATION STUDY OF THE INTERACTION BETWEEN THE PROPULSION AND FLIGHT CONTROL SYSTEMS OF A SUBSONIC LIFT FAN VTOL

Bruce E. Tinling
Ames Research Center

and

Gary L. Cole
Lewis Research Center

SUMMARY

The possibility of interactions between the propulsion and flight control systems of a three-fan subsonic VTOL aircraft has been studied using nonreal-time simulation. The objectives were to obtain time histories of critical internal engine parameters and to identify and analyze possible deleterious effects of engine dynamics on flight control. Analysis of the engine data was beyond the scope of the study.

The simulation results indicated no deleterious effects of engine dynamics on the control of the aircraft with the exception of the effects of the fan actuator deadband. A method of alleviating these effects through feedback of the actuator output to the flight controller was developed.

INTRODUCTION

During the critical transition and hovering flight phases, the propulsion system of a VTOL aircraft must provide control forces and moments as well as the forces necessary to sustain flight. Consequently, dynamic interactions between the propulsion and flight control systems are a possibility because logic to enhance handling qualities requires closed-loop control in which the propulsion system is an element of one or more high-gain control loops. Furthermore, the propulsion system must accommodate unique requirements such as power management between multiple engines and compensation for engine failures.

The handling qualities of VTOL aircraft with advanced controllers have been studied intensively, including real-time piloted moving-base simulations (see, e.g., refs. 1 and 2). In these studies, the propulsion system was approximated by a simple input/output relationship that represented the response to control inputs. This permitted an evaluation of the handling qualities in the powered-lift mode but did not provide information on the possibility of exceeding internal engine limits due to control activity. Further, the simple engine representation eliminates many possibilities of deleterious interactions between the dynamics of the engine and its control system and the flight control system. It is the purpose of the study to

examine these interactions for a subsonic VTOL aircraft with lift-cruise fans. The objective is to provide data from which it can be determined if a high-gain flight control system performs satisfactorily when the internal dynamics of the engine are represented and if control activity has an important impact on the engine design or life. Examples of the latter are excessive turbine temperature cycling and fan blade actuator activity.

The aircraft chosen for the study is a subsonic, three-fan VTOL design proposed as a research and technology aircraft. This design has been studied extensively in piloted simulations at Ames Research Center (see refs. 1 and 3). The propulsion system consisted of two turbofan engines, one turboshaft engine, and one remote lift fan. The fans were all connected with shafting through a gear box as illustrated in figure 1. The propulsion model was sufficiently detailed to permit monitoring of internal engine variables during transient operation. It included dynamic effects such as heat soak, rotor inertia, core speed control, and fan blade actuation.

The flight control system chosen for this study was the State Rate Feedback Implicit Model Follower described in reference 2. This controller provides an input/output relationship that approximates any selected second-order system; it provides good gust alleviation and cross-axis decoupling and is self trimming. This controller was chosen because it provides satisfactory handling qualities throughout a precision powered-lift instrument approach and in hovering flight. This performance is obtained through high-gain control loops that include the engine. Combining this controller with the detailed-engine model is therefore likely to expose dynamic interaction between flight control and engine dynamics existing for this type of aircraft.

The study was performed in nonreal-time digital simulation. The aircraft was required to follow a specified flightpath under automatic control in the presence of turbulence, initial vertical and lateral offsets, and engine failures. Example data are presented that illustrate the performance of the flight control system and the variation of critical engine parameters. A list of all of the flight conditions for the simulated approaches is included. The time histories of relevant parameters for these approaches have been recorded on magnetic tape and are available to agencies of the U.S. Government and its contractors upon request.

SIMULATION MODEL

The Navy research and technology aircraft was chosen for this study for several reasons. First, it represents a recent VTOL aircraft design for which a complete documented set of aerodynamic and design data is available (see ref. 3). Second, a digital computer program used for piloted simulation at Ames Research Center was readily available. Finally, and perhaps most important, a detailed simulation of a shaft-driven lift-fan propulsion system was available for this aircraft. This simulation was developed at Lewis Research Center.

Airframe

The aircraft (fig. 1 and table 1) was representative of a research aircraft with a wing span of 13.54 m and a gross weight of about 13,000 kg. Control in the powered-lift mode was provided through variable fan blade pitch, the thrust vectoring hoods and louvers, and attitude (see figs. 3 and 4). Pitch and roll control were provided through the variable pitch fans; yaw control through differential thrust vectoring; and lateral velocity control through roll of the aircraft. Lateral velocity control for low-speed flight was also available through thrust vectoring, but this mode was not used in this study.

Attitude and Flightpath Controllers

The attitude and flightpath controllers chosen utilize the principles of the state rate feedback implicit model following controllers described in reference 2. This approach was chosen for several reasons. First, it has been found to provide better handling qualities for the lift-fan aircraft than others which have been studied in simulation of VTOL aircraft at Ames Research Center (see ref. 2). Second, the high-gain controllers should require rapid response from the propulsion system, thereby exposing deleterious interactions. The controllers chosen for the study provided attitude command in pitch and roll, rate command with turn coordination in yaw (washed out at speeds below 20 knots), and vertical velocity and longitudinal acceleration command for control of the flightpath in the vertical plane. As previously noted, lateral flightpath control was provided through roll.

A curved decelerating approach was specified for the study, and command signals necessary to follow the trajectory were provided by a flight director directly coupled to the controllers. The elements of this flight director are described in reference 2. Signals were generated to command the roll angle for lateral flightpath control, and the attitude rate and longitudinal acceleration for longitudinal flightpath control. The pitch attitude was commanded to be zero degrees, which is considered to be the best touchdown attitude, for the entire trajectory.

Block diagrams of the state rate feedback implicit model following controllers are shown in figures 5 and 6. These controllers differ in detail from those shown in reference 2 in that the manual control provisions and alternative modes of operation have been deleted. In addition, the controllers for ϕ, θ, $\dot{h}$, and $\dot{V}_x$ have been modified to provide separate control signals to the aerodynamic and to the propulsive controls. Also, in those instances where control of the variable pitch fans is required, provision has been made for feedback from the actuators to the controller. The reasons for these latter modifications to the controllers will be developed in the discussion of the results.

Details of the power lever system, the engine speed control, and the fan blade actuation system are shown in figures 7, 8, and 9. These systems are similar to those employed in the piloted simulation study reported in reference 1 with the exception of the fan blade pitch actuators. These actuators

were assumed to have a deadband as illustrated in the lower part of figure 8. The magnitude of the deadband was nominally set at 0.5° and the actuator time constant at 0.1 sec.

The actuators for all aerodynamic controls had no deadbands and were modeled as described in reference 3. The time constant for these actuators was typically 0.1 sec.

The flight director and various elements of the flight and engine control systems require data on attitudes, rates, accelerations, engine speeds, and so on. For this study, all measurements to provide these data were assumed to be perfect.

Propulsion System

As indicated in the sketch of the aircraft in figure 1, the propulsion system consists of two turbofan engines, one turboshaft engine and one lift fan. The units are all connected with shafting through a gear box. The remote unit is disengaged by clutch during conventional flight. The core engines are modified Detroit Diesel Allison XT701-AD-700 engines and the fans are Hamilton Standard 1.57 m (62 in.) diameter variable-pitch, low-pressure ratio fans. Additional information concerning these units is given in reference 4.

The propulsion representation used in this model is nonlinear and considerably more detailed than that originally used for piloted real-time simulation. The major advantage of the detailed model is that it allows monitoring of internal engine variables (i.e., temperatures and pressures throughout the engine) during transient operation. The propulsion model includes dynamic representations of the rotor inertias, heat soak, the core speed controller and the fuel valve. Block diagrams of the propulsion system and core speed control are given in figures 2 and 8, respectively. Each propulsion unit has its own representation. However, only two representations are shown in figure 2 since units 1 and 2 are identical. The fuel controls for all three engines are identical.

The major inputs to the propulsion system are fuel flow (WFM) to each engine (output of the speed control and fuel valve of figure 8 which will be discussed later) and the fan pitch angles β_1, β_2, and β_3 (see fig. 9). Aircraft altitude ALT is input and is used to determine ambient temperature and pressure from standard atmosphere tables. Hot or cold days can be simulated by the input DTT (fig. 2). Ambient conditions (PO, TO) plus the aircraft Mach number MNO are used to compute free-stream total conditions from the compressible flow equations. The inlet pressure recovery was assumed to be 100% for all three inlets; therefore total conditions into the fan are the same as free-stream totals. Also input to the fan are rotor speed, NL, and fan pitch angle, BETAF.

The fans are represented by maps of total fan corrected airflow, pressure ratio and temperature ratio as functions of fan pitch angle (BETAF), and fan corrected speed. The maps are constructed according to the assumption that each fan operates along a single operating line depending on BETAF. The

fan maps cover the following ranges: fan corrected speed, 70 to 110%; and fan pitch angle, -20 to +7.3°.

Separate temperature and pressure ratios are calculated for the hub (station 25) and tip (station 13) of fans 1 and 2. Inputs to the compressor are total pressure and temperature (PT25, TT25) from the fan and high-pressure rotor speed NH. The compressor is represented as single operating lines of efficiency and corrected airflow as functions of corrected speed. Values are mapped for corrected speed in the range of 65 to 107.5%. Actual compressor airflow W25 was calculated and subtracted from total fan air W1 (propulsion units 1 and 2 only) to give the fan duct airflow (WA13).

The fan duct is simply treated as a constant total pressure loss resulting in PT18. Inputs to the combustor are pressure PT3, temperature TT3 (which is the output of compressor heat-soak lead-lag dynamics), airflow W3, fuel flow WFM (output of the fuel valve, fig. 8) and the compressor exit static pressure PS3. The combustor generates a temperature TT4P and a function of airflow W3, fuel flow WFM and temperature TT3. The high-pressure turbine inlet temperature TT4 is the output of turbine heat-soak lead-lag dynamics, and PT4 is assumed to be equal to PS3. The calculation of PS3 requires an iteration process. Pressure PT42 and temperature TT42 out of the high-pressure turbine are assumed to be directly proportional to PT4 and TT4, respectively. Temperature, pressure, and flow at the nozzle for units 1 and 2 are calculated assuming mixing of the duct and low-pressure turbine airstream.

The gross thrust FGROSS is calculated from conservation of momentum using WG18 and V18 (which depends on TT18 and PT18). In the case of propulsion units 1 and 2, the nozzle air temperature is higher than that from the fan duct alone because of mixing with the hot core air. The higher temperature results in higher thrust than would be obtained from airflow at the lower fan duct air temperature. In the case of propulsion unit 3, only the fan is assumed to produce thrust (core thrust is negligible). The gross thrusts are output to the aircraft simulation along with inlet airflows for the calculation of net thrusts.

Rotor speeds NH and NL are determined from the power absorbed by the compressor HP2C or the fan HPF and the power output by the corresponding turbine (HP2T or HP1T). In the case of the fans, since all three are connected by shafting, the HPF's and HP1T's are summed as shown in figure 2. The time rate of change of speed NL is directly proportional to the ΔHP's and inversely proportional to rotor inertia $3I_{LP}$ and rotor speed NL. $\dot{NL}$ is integrated to obtain NL which is the same for all three fans. Although not shown in figure 2, an option is available to allow declutching of the nose fan (no. 3). In that case, the power absorbed by fan 3 HPF3 and the inertia of fan 3 go to zero.

High-pressure rotor (compressor) speed NH is determined in the same manner except that each rotor works independently. Therefore, NH's are not necessarily the same. For simulation of a core failure, the power output of the associated low-pressure turbine HP1T goes to zero. Also, the temperature of the nozzle flow is set equal to the fan duct air temperature (i.e., no heating from core).

Core Speed Control Details

A block diagram of the engine core speed control is shown in figure 8. Included are the dynamics of the compressor-inlet total-temperature (TT25) sensor and the fuel metering valve. Both are first-order lags. The inputs to the fuel control are sensed compressor inlet temperature T25SN, compressor exit static pressure PS3 (i.e., the sensor is assumed to be perfect — no dynamics), high-pressure rotor mechanical speed NH and demanded high-pressure rotor corrected speed PCNHD. The demanded speed for each engine is determined from the fuel flow demanded by the power lever system by an equation of the form PCNHD = C_1*(PCNHC)**0.2 + C_2 (C_1 and C_2 are constants but different for different engines) (see upper part of fig. 8). The fuel control incorporates a proportional-plus-integral controller and acceleration and deceleration schedules. The control limits engine operation between mechanical speeds of 57% and 110%. The output of the fuel valve WFM goes to the combustor as shown in figure 2.

SIMULATED FLIGHT CONDITIONS

The flight conditions for the digital simulation were specified to permit study of the following on the response of the aircraft and its propulsion system:

- Initial localizer and attitude errors
- Engine failures
- Gross weight (minimum 11,000 kg; maximum 12,960 kg)
- Ambient temperature (standard day 15°C; hot day 32.2°C)
- Turbulence level (0.25 m/sec to 2 m/sec rms)
- Fan blade angle deadband
- Fan blade actuation time constant
- Methods for alleviating effects of fan blade actuation deadband

A complete list of the simulated approaches is given in table 2.

For all of the data, the same commanded trajectory and wind conditions were specified. The trajectory consisted of a curved decelerating approach that was initiated at an altitude of about 460 m on a three-degree glideslope. The commanded deceleration was constant except for the first few seconds and the last few seconds prior to hover. The data records taken consist of approximately the last 120 sec of the approach. The heading was 90° in all cases with a 20-knot mean wind from 60°. Turbulence was introduced for all cases, since it was found that under some conditions a small disturbance was required to induce attitude oscillations caused by the fan blade actuator deadband. The lowest level of turbulence used was 0.25 m/sec rms. The wind model used and the Dryden turbulence model are defined in MIL-F-8785B (see ref. 5). The random number sequence used in generating the turbulence was identical for all trajectories so that the results are directly comparable.

RESULTS AND DISCUSSION

Typical Results

An example of typical results obtained from the simulation is given in figure 10. For this set of data, the gross weight was set at the maximum (12,960 kg), the ambient temperature corresponded to a hot day (32.2°C), a 20-knot wind was imposed at an angle of 30° from the flightpath with an rms turbulence level of 1 m/sec, and an engine failure was introduced at an attitude of about 305 m. In addition, the initial altitude and lateral positions were displaced 20 m from the commanded flightpath. For these results the actuator deadband was zero. The results indicate excellent flightpath tracking with an altitude loss at the time of the engine failure of only 0.6 m. The time histories of the internal propulsion system parameters show the dynamic response to turbulence and to engine failure. Note that, with one engine inoperable, the peak temperature at the burner outlet of the operating engines reaches about 1620 K when velocities approaching hover are reached. This is the temperature specified for the one-hour contingency rating in the engine design (see ref. 6).

A complete list of conditions for which similar data were obtained is given in table 2. These results do not include the final deceleration to hover. Results that are limited to approximately the last 20 sec prior to hover and which include the effects of temperature rise due to reingestion are discussed in a subsequent section. A complete list of the conditions for which these results were obtained is given in table 3.

Effects of Fan Blade Actuator Deadband

A characteristic of hydraulic actuators is that some deadband will exist, the magnitude depending on the particular design. A block diagram representing the dynamics of the fan blade pitch actuator with its deadband is shown in the lower part of figure 9. Note that the output of the actuator is an input to the engine model, and therefore the actuator deadband can be easily included in simulations using either a detailed engine model or a simpler representation such as used for piloted simulation (ref. 3). The effective actuation time constant caused by the deadband will depend on the magnitude of the command signal, being relatively small for large inputs, and becoming infinite for infinitesimal signal inputs. For this study, a nominal deadband of 1/2° was assumed.

The effect of the deadband on the angular acceleration and on the fan blade pitch actuation is shown in figure 11. For this approach, mild turbulence was imposed to provide a continuous disturbance. It would be anticipated from the nature of the turbulence model and from the decreasing flight speed that the envelope of the angular accelerations would decrease as the approach continued, as was the case with zero deadband shown in the upper right part of figure 10b. When the fan blade actuation deadband is present and the airspeed has decreased to about 60 knots (time ≈70 sec), a high-frequency oscillation in attitude occurs that is caused by a limit-cycle

oscillation of the fan blade pitch actuators. This activity can be more clearly seen in figure 11b, where the actuator command signal and actuator position are shown on an expanded scale. This oscillation does not cause any appreciable deviation in the commanded attitude or flightpath but would certainly be annoying to a pilot, might induce resonant oscillations of the aircraft structure, and would decrease the service life of the actuators.

The limit-cycle oscillation is a consequence of the low airspeed and the attendant decrease in aerodynamic damping. This damping must be provided by the control system, requiring the fan blade actuators to follow small inputs. This limit-cycle oscillation can be demonstrated for a much simpler system than the lift-fan aircraft and its control system (see fig. 12). The controlled element in this case is a first-order rate damped system representative, for example, of single degree of freedom roll control of a conventional airplane. The controller is a simple state rate feedback implicit model follower developed using the same principles described in reference 2. For sufficiently high values of the gain K, the overall transfer function will be that of a simple rate damped system with a time constant $1/K_1$ regardless of the value of the damping parameter D_1, providing that the actuator dynamics can be approximated as $1/(\tau_a S + 1)$. However, when a deadband is present in the actuator of the type assumed for the lift-fan aircraft and the damping of the plant is low, the response of the system to a small pulse consists of a limit-cycle oscillation as illustrated in figure 12.

It was shown in reference 2 that the path 1-2 in figure 12 must contain a dynamic element to be physically realizable. Further, it was shown for a linear system that representation of the actuator dynamics in the path 1-2 yields the desired system response. This result leads heuristically to an attempt to regain the desired performance for a system with a deadband in the actuator by placing a model of the actuator, inducing the deadband in the path 1-2. The results of such an experiment are shown in figure 13. It is shown that this approach eliminates the limit-cycle oscillation, although the response differs from the desired linear transfer function represented by $x/x_c = K_1/(s + K_1)$. However, for inputs equal or larger in magnitude to the deadband little difference from the desired linear response can be observed.

Propulsion/Control System Integration to Suppress the Effects of Fan Blade Pitch Actuator Deadbands

Application of the heuristic approach to suppress the effects of the actuator deadbands is more complicated than for the simple system described in the preceding section. The controller, as developed in reference 2, controls both the aerodynamic and the propulsive forces and moments. Application of the technique indicated by the study of the simple system requires that a model of the actuator be in the controller for each force or moment generator; otherwise, limit-cycle tendencies were found to exist because the activity of all actuators was not properly modelled. This requirement leads to developing the roll, pitch, and vertical flightpath controllers into branches (figs. 5 and 6) so that appropriate actuator dynamics can be inserted in each. Further, there is a possibility that the commands to the aerodynamic and propulsive actuators will diverge, yielding opposing control moments. This is prevented

in the long term through an interconnect between the branches which has a sufficiently long time constant so as not to interfere with the short period dynamics. When the airspeed becomes sufficiently low, it is necessary to eliminate inputs to the aerodynamic controls since their activity further excites limit-cycle oscillations at these speeds.

The success of the above modifications in eliminating the limit-cycle oscillations can be described as erratic. There is nothing in the mechanization of the actuator model to guarantee that it is operating synchronously with the actuators. Accordingly, under some conditions, the mechanization reduced the level of the oscillation; under others, the oscillations increased. One of the latter cases is shown in figure 14. It can be seen that, compared to the uncompensated case, the pitch frequency is reduced and the amplitude is increased over the final 20 sec of the approach. These two changes are likely to be deleterious to piloted operation since there is sufficient time during an oscillation to reach attitude errors of the order of a degree, and the frequency is sufficiently low for the pilot to attempt corrective control — possibly leading to pilot-induced oscillations.

For the simple single degree of freedom system discussed earlier, the obvious solution in overcoming the deficiencies of the actuator model approach is to remove the actuator model from the controller and replace it with the output signal from the actuator itself multiplied by 1/K (see fig. 12). This ensures that the input to the controller and the actuator are synchronized. An additional advantage is that the actuator is likely to require a far more complex representation than the simple form shown in figure 9, and accurate modeling might be difficult or at least an unwanted complication. The feedback of the actuator output to the controller eliminates this complication as well as ensures that the controller is receiving correct information.

For the aircraft controller, the solution is not as straightforward. As indicated in figure 9, the signals are mixed, each actuator being driven by a linear combination of the signals from each controller, that is:

$$\begin{vmatrix} \text{BETN1} \\ \text{BETN2} \\ \text{BETN3} \end{vmatrix} = [M] \begin{vmatrix} \delta_{v_\beta} \\ \delta_\theta \\ \delta_\phi \end{vmatrix}$$

when M is the matrix of gains in the signal mixing logic. Estimates of the quantities to be fed back that indicate the effects of actuator lags and deadbands were obtained by multiplying the inverse of M by the output of the actuators; that is,

$$\begin{vmatrix} K_{v_\beta}\hat{\delta}_{t_\beta} \\ K_\theta\hat{\delta}_\theta \\ K_\phi\hat{\delta}_\phi \end{vmatrix} = [M^{-1}] \begin{vmatrix} \text{BETAF1} \\ \text{BETAF2} \\ \text{BETAF3} \end{vmatrix}$$

The quantities K_{v_β}, K_θ, and K_ϕ represent the gains between the input to the signal mixer and the points at which $\hat{\delta}_{t_\beta}$, $\hat{\delta}_\theta$, and $\hat{\delta}_\phi$ are fed back to the controller, replacing the signal from the actuator model in each case (see figs. 5 and 6). This computation obviously cannot provide perfect information because of the inherent characteristics of the deadbands and actuator lags and will result in some coupling between the various controllers. Despite these imperfections and coupling, use of this technique met with considerable success as indicated in figure 15. It can be seen that the magnitude of the angular oscillations and the actuator motion are considerably reduced compared to the cases with no compensation or with model compensation.

The integrated controller, using blade actuator signals fed back from the engine, was found to be tolerant of changes in actuator dynamics. An example is shown in figure 16, where it has been assumed that the time constant of the actuators will depend on whether the blade angle is increasing or decreasing. This difference in time constant is a possibility because of the presence of aerodynamic torques on the blades (see ref. 4). For the case shown in figure 16, it is assumed that the time constant for increasing the blade angle will be 0.3 sec, three times the nominal value of 0.1 chosen for the study. The results show some increase in the angular oscillations, but the resulting pitch and roll oscillations due to the actuator activity remains well below 1° amplitude.

The effect of all changes to the blade actuator system studied are summarized in figure 17. These results are all for light turbulence and consist of maximum angular acceleration recorded during the time interval for the approach from 5 to 105 sec. The advantage of the feedback type mechanization in reducing the maximum pitch accelerations is clearly evident as is the decrease in performance when the time contant for increasing blade angles is tripled. A further doubling of the time constants for both increasing and decreasing blade angles roughly triples the maximum angular accelerations.

With feedback compensation, changes in the deadband characteristics did not produce any large changes in the maximum angular acceleration. With no deadband compensation, a reduction in the deadband by a factor of 2 to 0.25° was found to reduce the motion by a factor of about 2. However, as indicated in figure 17, reducing the deadband caused only a small improvement for the compensated system. It was also found that different deadbands for each actuator, averaging to the nominal value of 0.5° (0.25°, 0.75°, and 0.50°), had negligible effect on maximum accelerations.

In addition to the motion caused by actuator dynamics, the response of the compensated systems to increasing turbulence level was examined. These results are summarized in figure 18. If these results are extrapolated to zero turbulence, it can be seen that the increment contributed by the effects of fan blade pitch angle deadband are generally small compared to the overall effect of turbulence on angular accelerations. Further, the rate of increase of angular acceleration with increasing turbulence for no deadband compensation or with feedback compensation differs little from that with zero deadband. This implies that the excellent response to turbulence of the state rate

feedback implicit model following controller (ref. 2) is retained in the presence of fan actuator deadband.

The flightpath performance showed no important variation for any of the controller configurations studied. For the lowest turbulence level (0.25 m/sec rms), the maximum attitude error was less than 0.11 m; for a turbulence level of 2 m/sec, this error was always less than 0.6 m.

Effects of Temperature Rise Due to Engine Exhaust Reingestion

The effects of reingestion were studied in the final stage of the approach to a hover. The commanded hover altitude was set at 4 m to ensure that the maximum effect of the temperature rise would be experienced. In practice it is unlikely that the approach trajectory would terminate at such a low altitude; instead hover would be established at a considerably higher altitude followed by a vertical descent to a landing.

The temperature increase due to engine exhaust reingestion was estimated from the test results given in reference 7. The temperature rise index employed is shown in the upper part of figure 19. Data were not available from which to establish the temperature rise at a location corresponding to the inlet of the turboshaft engine mounted in the fuselage of the simulated aircraft. It was assumed that this temperature was identical to that at the inlet to the nose fan. This assumption was thought to be as realistic as any other and had the advantage of requiring a minimum of modification to the simulation. It should be noted that the data on which the temperature increases are based was obtained during a static test. Thus, no dynamic effects are included (e.g., horizontal or vertical velocities that exist for the trajectories studied). The results shown, therefore, represent a worst case situation since motion of the aircraft or any relative ind would preclude the temperature from reaching steady state levels.

Ground proximity also usually has an aerodynamic effect on propulsive lift. For this simulation, no such ground effect was assumed.

The temperature variation at the inlet for a typical approach is shown in the lower part of figure 19. The curves have a somewhat different shape from those in the upper part of the figure since ingestion causes a positive feedback whereby the temperature of the exhaust gases continues to increase as the height decreases to about 4 m, causing a greater rate of increase of inlet temperature.

Simulation results were obtained for two approach types: the 3° curved approach and the 3° straight approach. In each case, the number two engine was assumed to have failed. The curved approach required a 0.61 m/sec^2 vertical acceleration to be reached during the last 8 sec to achieve hover. In the presence of an engine failure, this could not be achieved for gross weights greater than about 11,000 kg. The 3° straight approach does not require a deceleration normal to the flightpath, allowing a somewhat greater gross weight of 11,700 kg. The variation of altitude, net thrust, and turbine inlet temperature for each of the two approaches, with and without reingestion, is

shown in figure 20. For these results wind and turbulence are assumed to be zero. As can be seen, for either approach, the reingestion temperature rise causes a decrease in the net thrust and a consequent loss in altitude of 2 to 3 m before the controller could arrest the rate of sink. Also the turbine inlet temperature rise on the order of 120 K is imposed on the already elevated temperature as a consequence of the engine failure. The maximum temperature reaches about 1700 K or about 80 K in excess of the temperature stated in reference 6 as the 1 hr contingency rating.

CONCLUDING REMARKS

A nonreal-time digital simulation of a lift-fan VTOL aircraft with a detailed representation of the propulsion system has been employed to study interactions between the propulsion and flight control systems. In addition, the detailed propulsion system representation provided information useful for propulsion system design (e.g., temperature cycling data which may affect engine fatigue life).

The results of the study indicated no deleterious effects of engine dynamics on the flight dynamics that could not be established using a much simpler engine model developed for real-time piloted simulation. The only deleterious effect observed on flight dynamics was caused by the deadband in the fan blade pitch actuators — an effect that can be included easily in the simpler propulsion system representation. A technique was developed for alleviating the effects of this deadband through feedback of the actuator signals to the flight control system.

Data were obtained documenting the response of critical internal engine parameters during an approach under autopilot control. Included are results that document the response to turbulence and engine failure and the effects of changes in ambient temperature and gross weight. These data are available on magnetic tape to agencies of the U.S. Government and their contractors.

REFERENCES

1. Bland, M. P.; and Konsewicz, R. K.: Simulator Results for Lift/Cruise Fan Research and Technology Aircraft. NASA CR-137979, Dec. 1976.

2. Merrick, Vernon K.: Study of the Application of an Implicit Model Following Flight Controller to Lift Fan VTOL aircraft. NASA TP-1040, Nov. 1977.

3. Bland, M. P.; and Konsewicz, R. K.: Mathematical Model for Lift/Cruise Fan V/STOL Aircraft Simulator Programming Data. NASA CR-151916, Dec. 1976.

4. Preliminary Design of Propulsion System for V/STOL Research and Technology Aircraft. NASA CR-135207, Mar. 1977.

5. Chalk, C. R.; Neal, T. P.; Harris. T. M.; Pritchard, F. E.; and Woodcock, R. J.: Background Information and Users Guide for MIL-F-8785B(ASG) Military Specifications — Flying Qualities of Piloted Airplanes. AFFDL-TR-69-72, Aug. 1969.

6. Definition of Propulsion System for V/STOL Research and Technology Aircraft. NASA CR-135161, Jan. 1977.

7. Schuster, E. P.; Carter, T. D.; and Esker, D. W.: Investigation of Ground Effects on Large and Small Scale Models of a Three Fan V/STOL Aircraft Configuration. NASA CR-152240, July 1979.

TABLE 1.- AIRCRAFT DIMENSIONAL AND MASS DATA

Wing span	13.54 m
Wing area	31.79 m^2
Empty weight	10,886 kg
Fuel load	2,041 kg
Moments of inertia, full fuel load	
I_x	30,973 kg m^2
I_y	53,971 kg m^2
I_z	67,841 kg m^2
I_{xz}	3,022 kg m^2
Engine thrust	151,057 N
Thrust-to-weight ratio — all engines operating	1.19

TABLE 2.- LIST OF SIMULATED APPROACHES

Approach number	Turbulence m/sec, rms	Engine failure number	Fan actuator deadband, deg	Deadband compensation	Other
1	1.00	2	0	---	Initial altitude error = 20 m; initial localizer error = 20 m
2	.25	No		---	
3	1.00			---	
4	2.00			---	
5	.25		0.5	None	
6	1.00			None	
7	2.00			None	
8	.25			Model	
9	1.00			Model	
10	2.00			Model	
11	.25			Feedback	
12	1.00				
13	2.00				
14	.25	2			
15	1.00	2			
16	2.00	2			
17	2.00	3			
18	2.00	2			Ambient temperature for standard day, 15°C
19	.25	2			Initial weight, 11,138 kg
20	2.00	2			Initial weight, 11,138 kg
21	.25	No			Fan blade actuator time constant for increasing blade angle, 0.3 sec
22	2.00				Fan blade actuator time constant for increasing blade angle, 0.3 sec
23	.25				Fan blade actuator time constant for increasing blade angle, 0.6 sec; decreasing 0.2 sec
24	2.00				Fan blade actuator time constant for increasing blade angle, 0.6 sec; decreasing 0.2 sec
25	.25		.25		
26	2.00		.25		
27	.25		Variable		Deadband #1, 0.25; #2, 0.75; #3, 0.50
28	2.00		Variable		Deadband #1, 0.25; #2, 0.75; #3, 0.50

TABLE 2.- CONCLUDED

Note: The following conditions existed for all approaches, unless specified differently in the column designated "other."

Flightpath	Curved decelerating approach, ψ = 90° — see figure 10
Wind	20 knots, from ψ = 60°
Initial gross weight	12,960 kg
Ambient temperature	32.2°C (hot day)
Fan blade actuator time constant	0.1 sec
Initial altitude and localizer errors	0
Altitude for engine failure	305 m

TABLE 3.- LIST OF APPROACHES TO HOVER

Approach number	Type	Gross weight	Engine failure number	Reingestion
1	3°-curved	12,800	No	Yes
2	↓	12,800	No	No
3	↓	11,010	2	No
4	↓	11,010	↓	Yes
5	↓	12,860	↓	No
6	3°-straight	12,860	↓	Yes
7	3°-straight	11,690	↓	Yes
8	3°-straight	11,690	↓	No

Note: All approaches are with blade actuator deadband of 0.50 and with feedback compensation. No wind or turbulence.

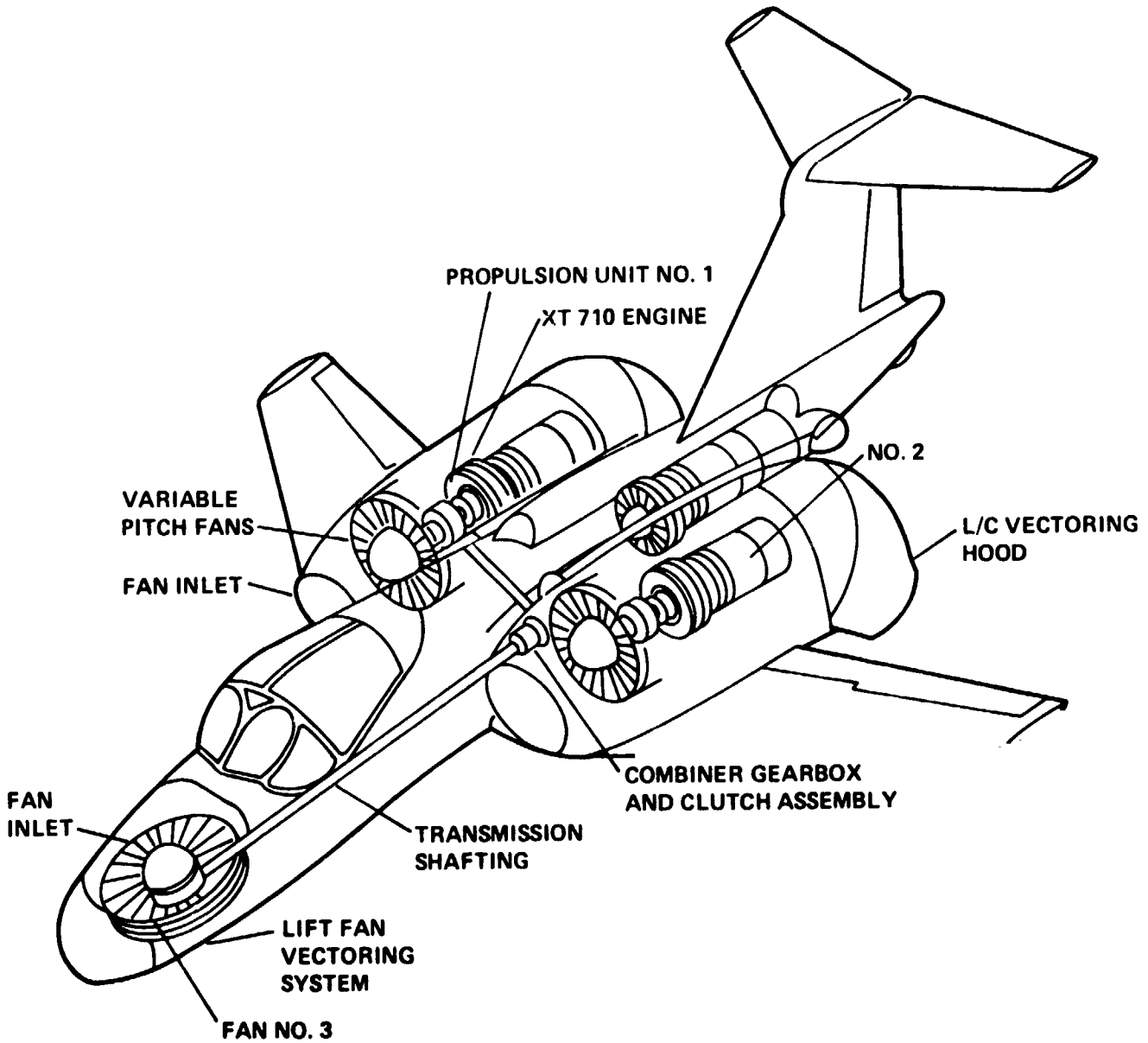

Figure 1.- Sketch of simulated lift-fan aircraft.

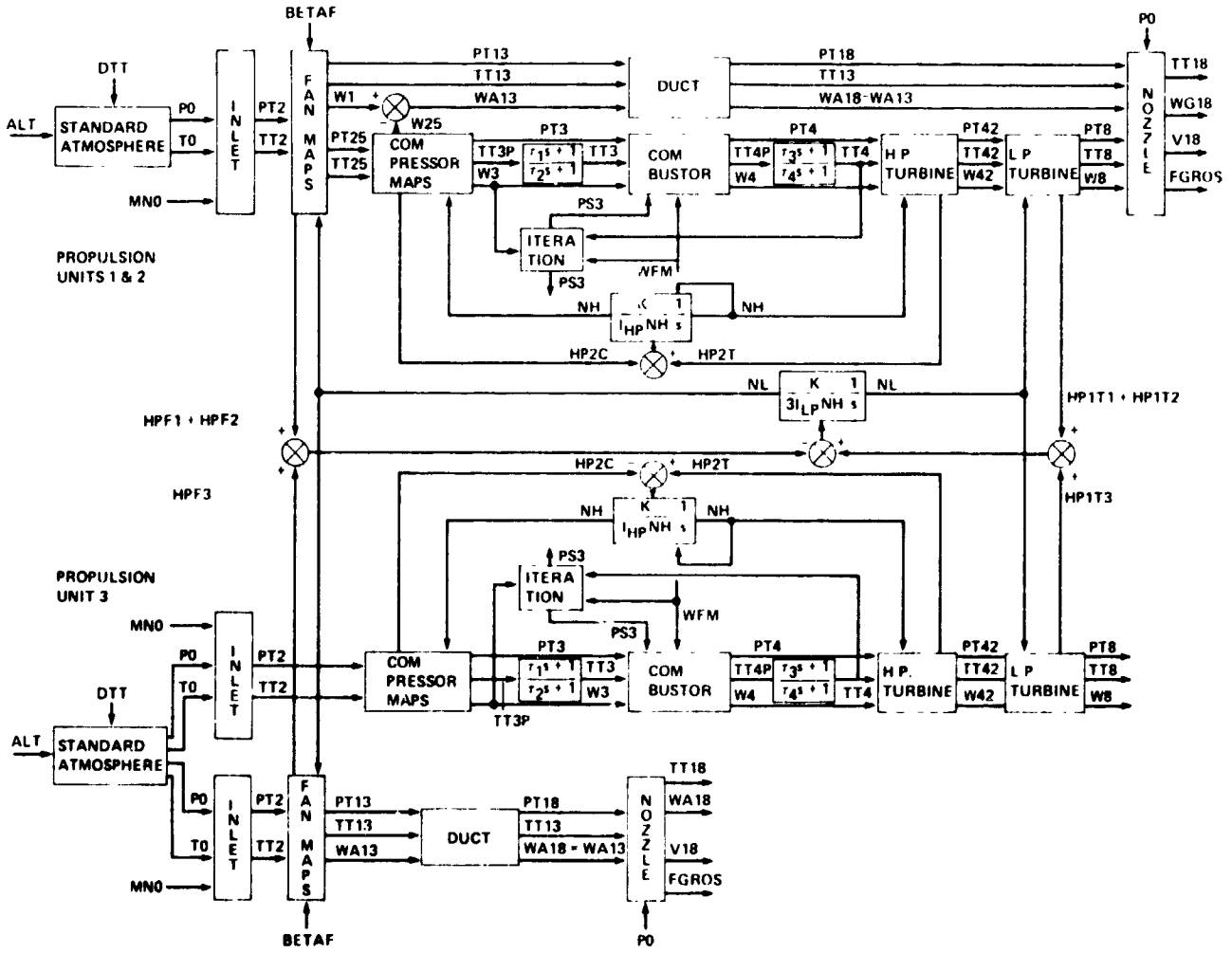

Figure 2.- Block diagram of engine model.

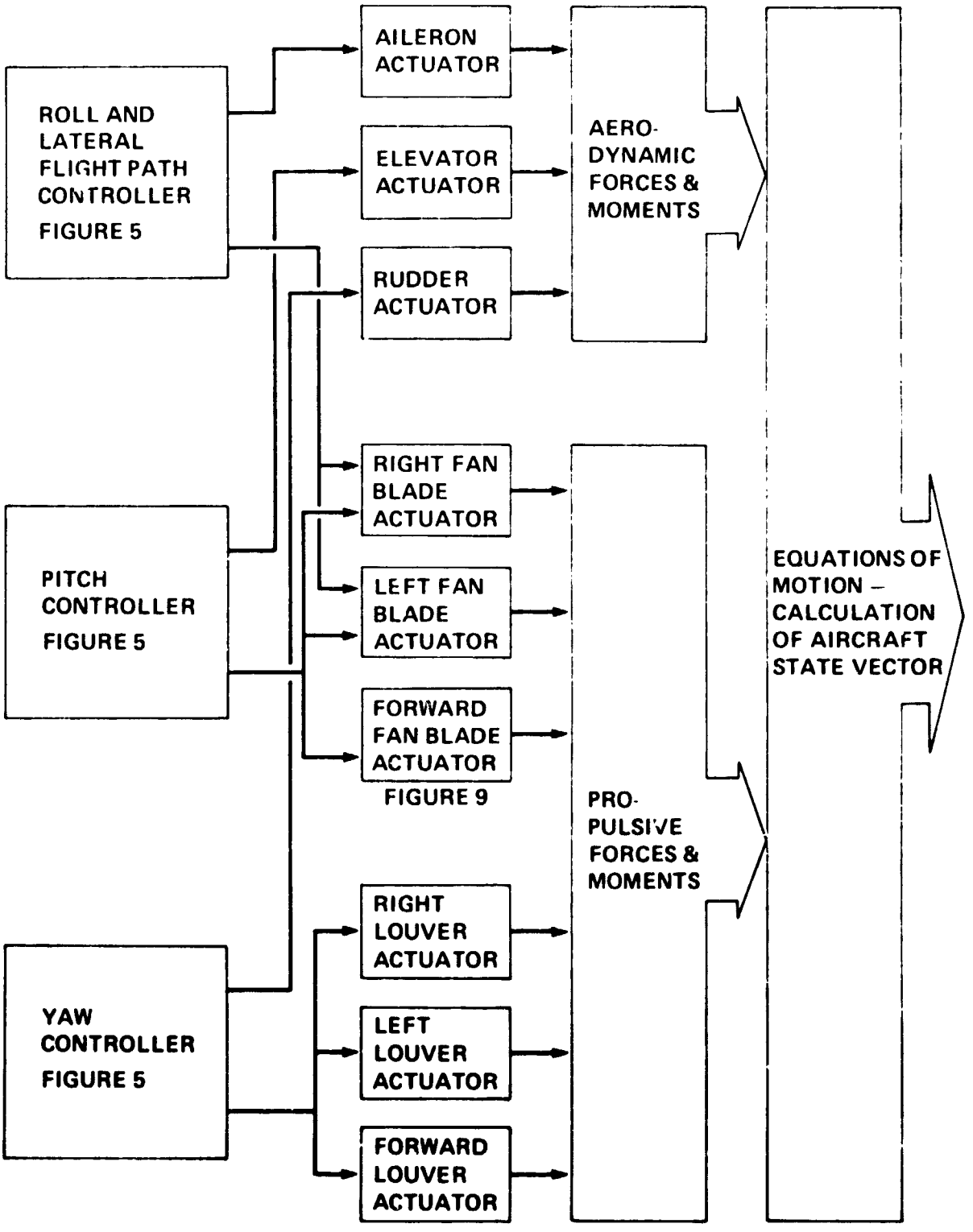

Figure 3.- Attitude control schematic.

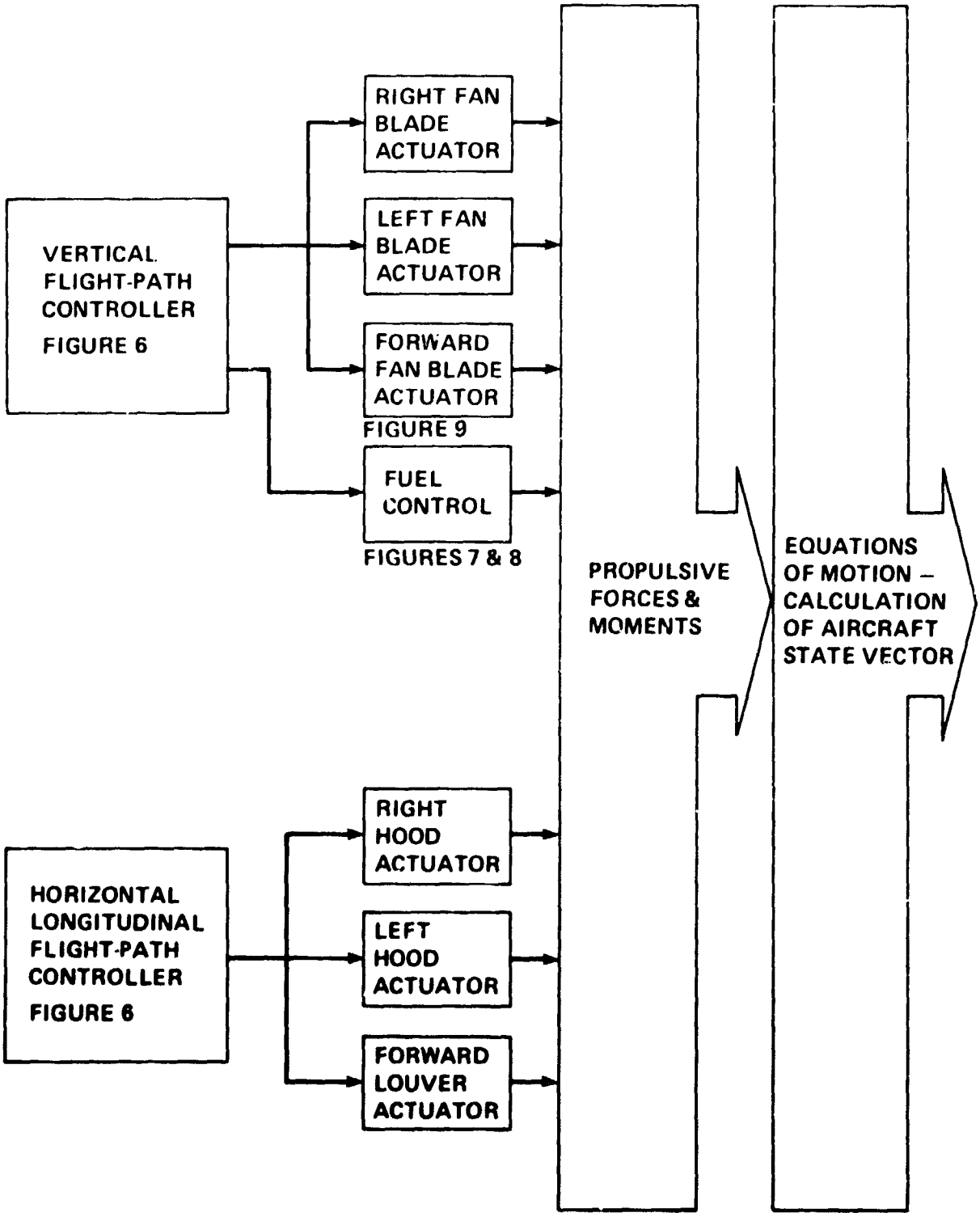

Figure 4.- Flightpath control schematic.

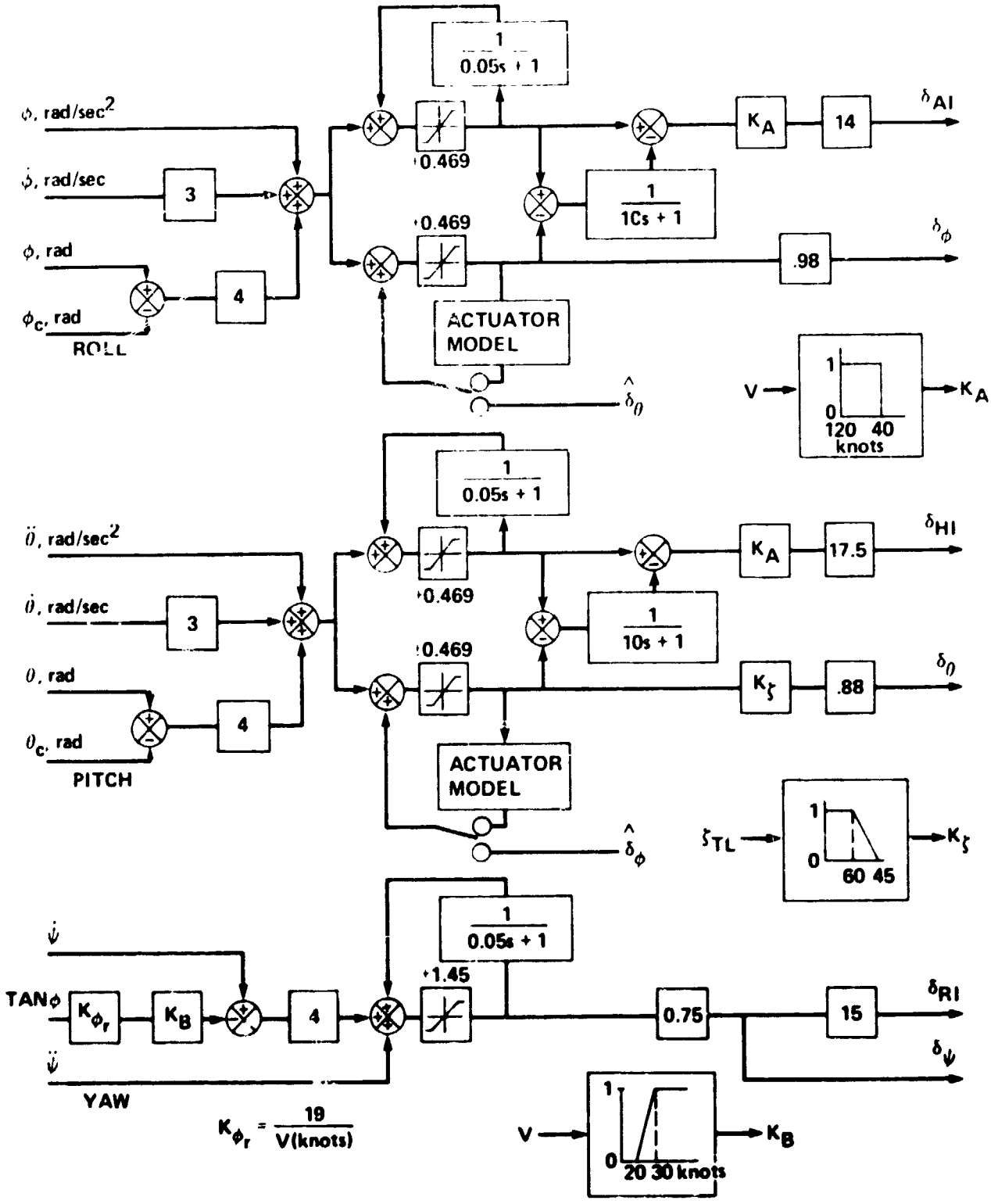

Figure 5.- Block diagram of attitude controller.

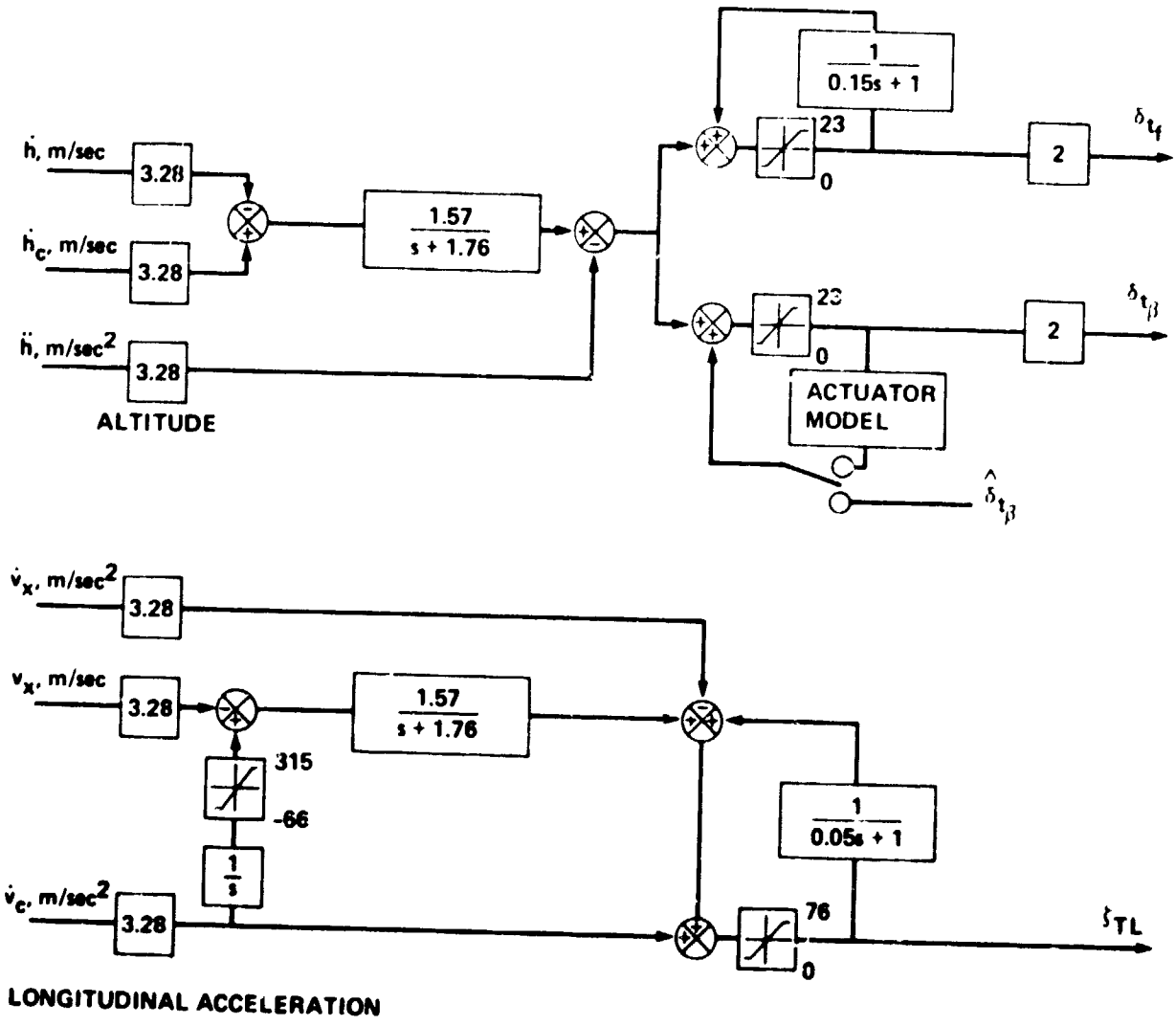

Figure 6.- Block diagram of flightpath controller.

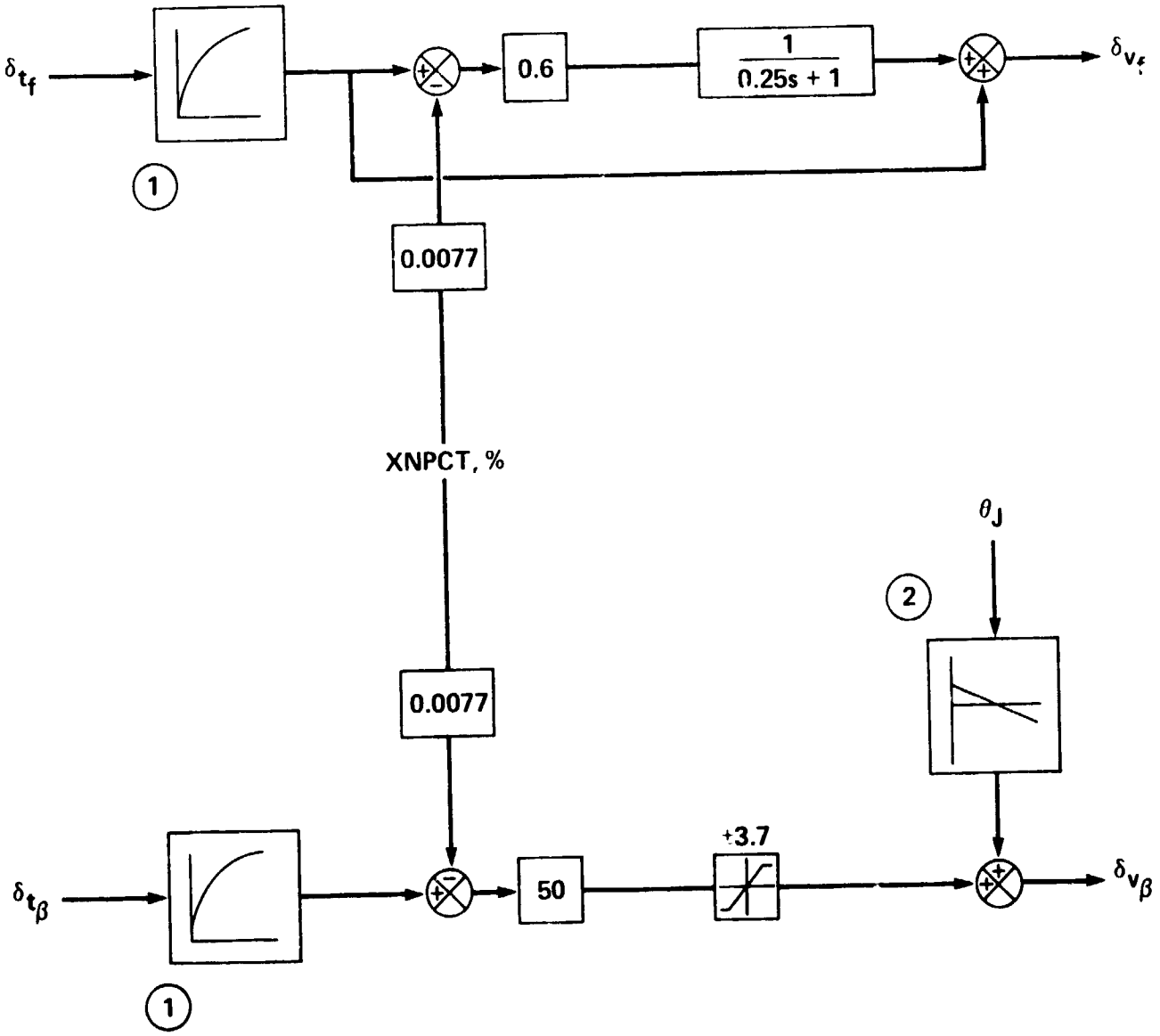

(1) HEIGHT CONTROL INPUT SCHEDULE

(2) BLADE ANGLE BIAS SCHEDULE

Figure 7.- Power lever system

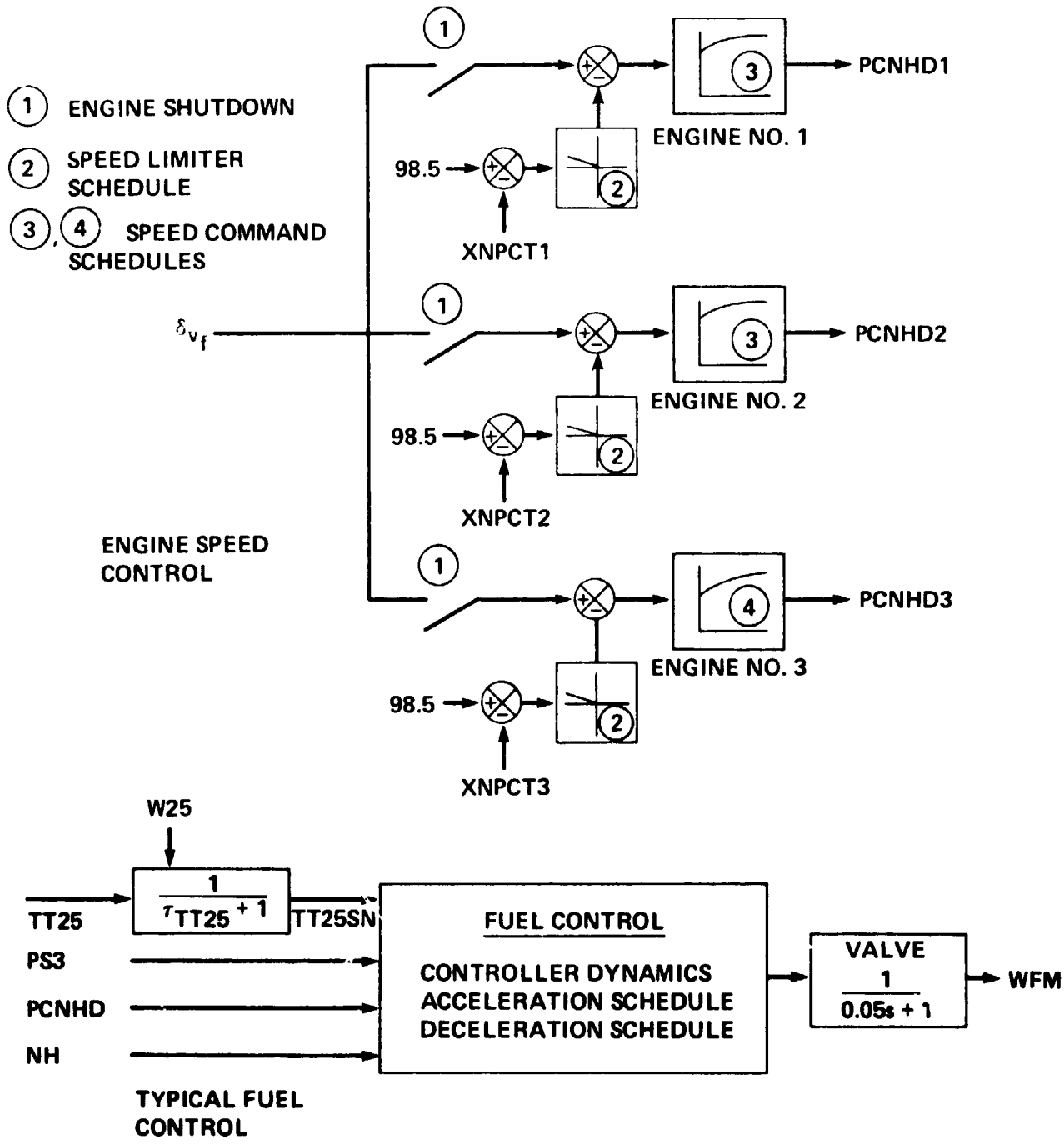

Figure 8.- Fuel and engine control details.

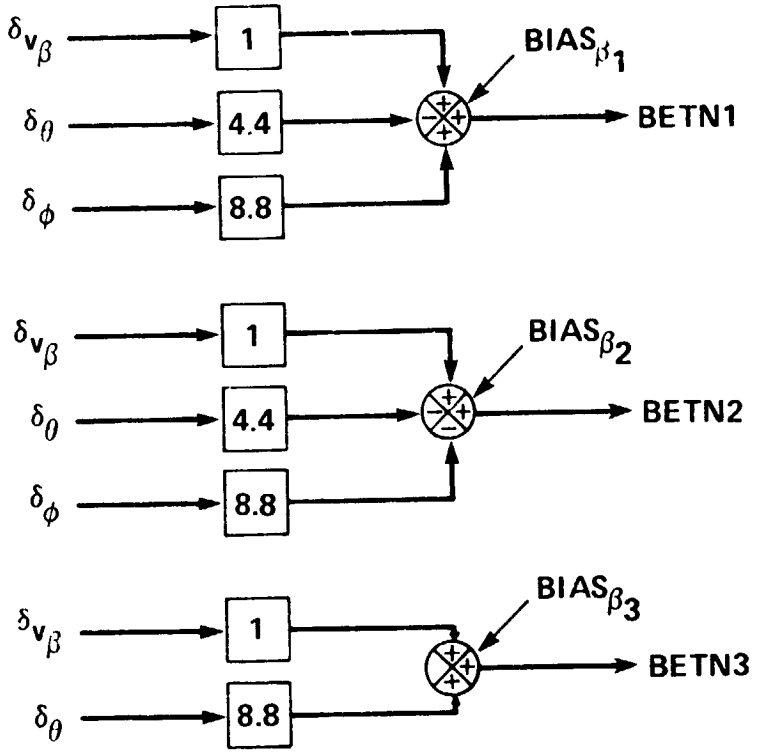

SIGNAL MIXING

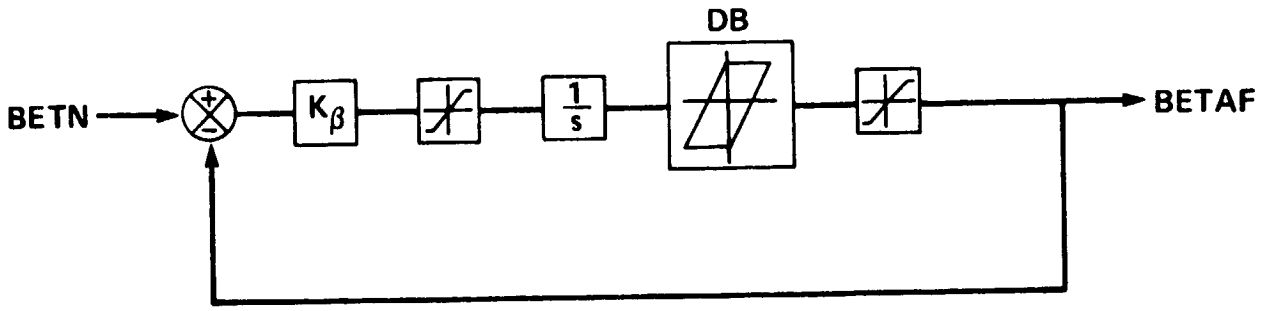

TYPICAL ACTUATOR

Figure 9.- Fan blade pitch actuation details.

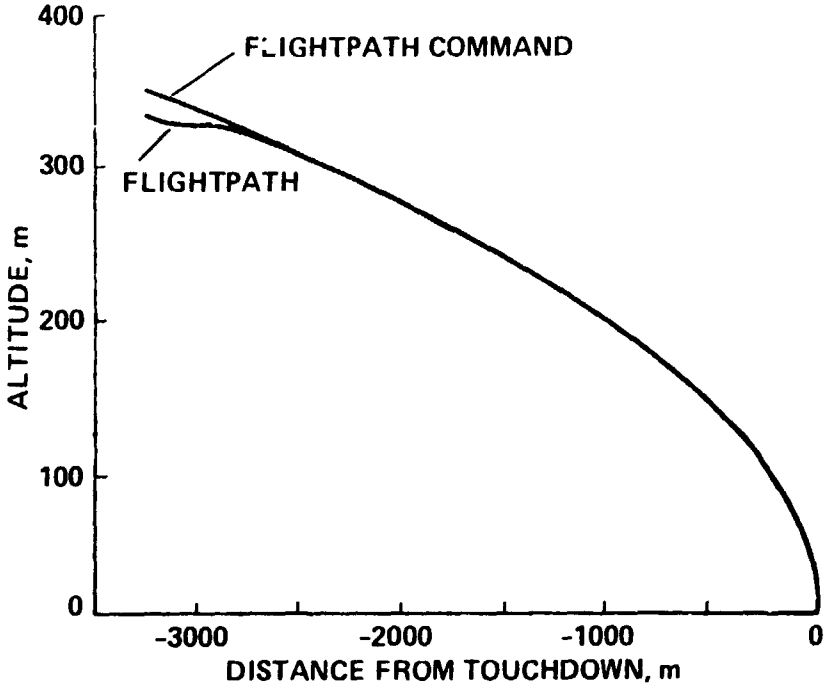

(a) Flightpath.

Figure 10.- Airframe and engine data for a typical approach. Conditions: maximum gross weight, 20-knot wind 30° from flightpath heading (ψ = 90°), 1 m/sec rms turbulence, hot day, failure of no. 2 engine at 300 m altitude, no fan actuator deadband.

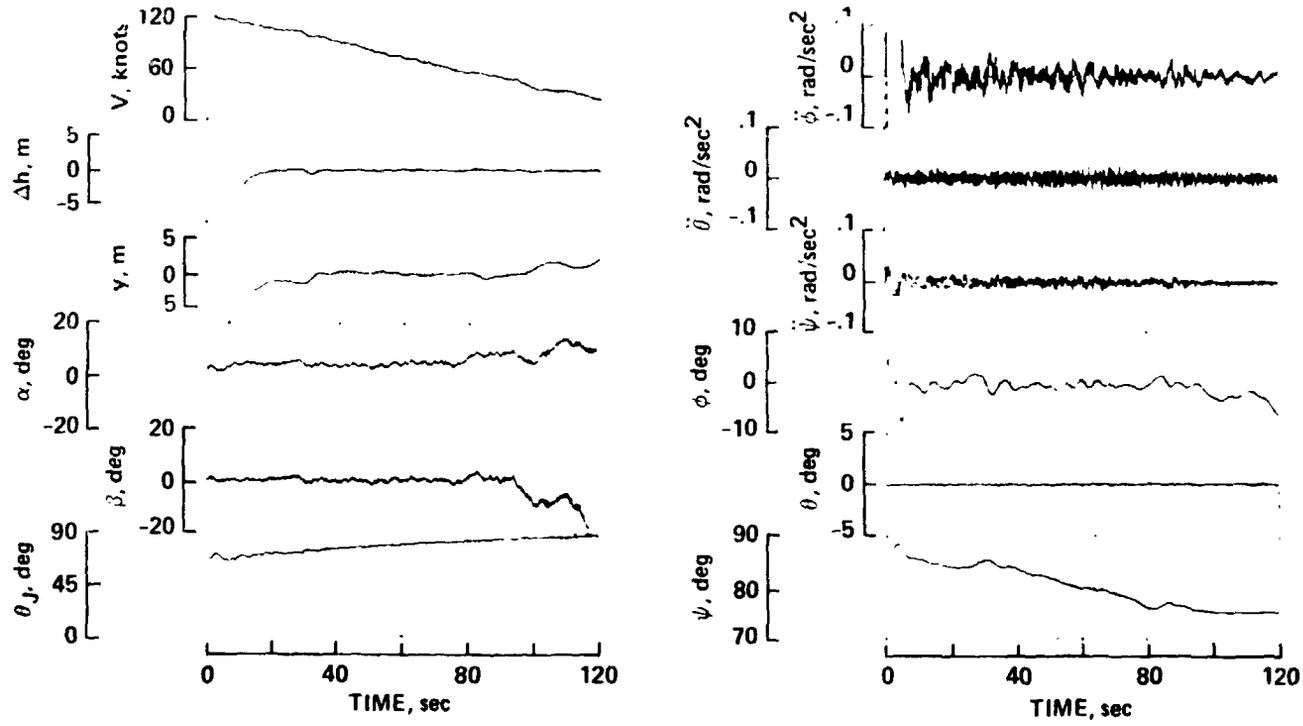

(b) Airframe variables.

Figure 10.- Continued.

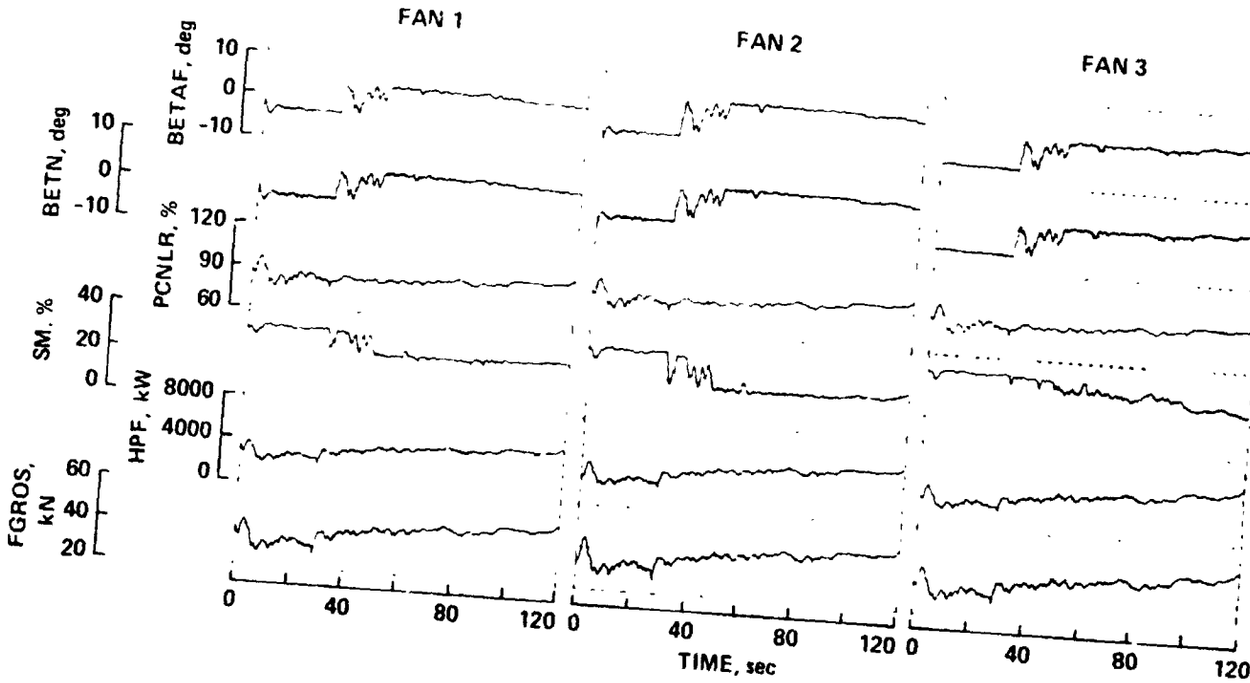

(c) Fan variables (engine no. 2 failure at 28 sec).

Figure 10.- Continued.

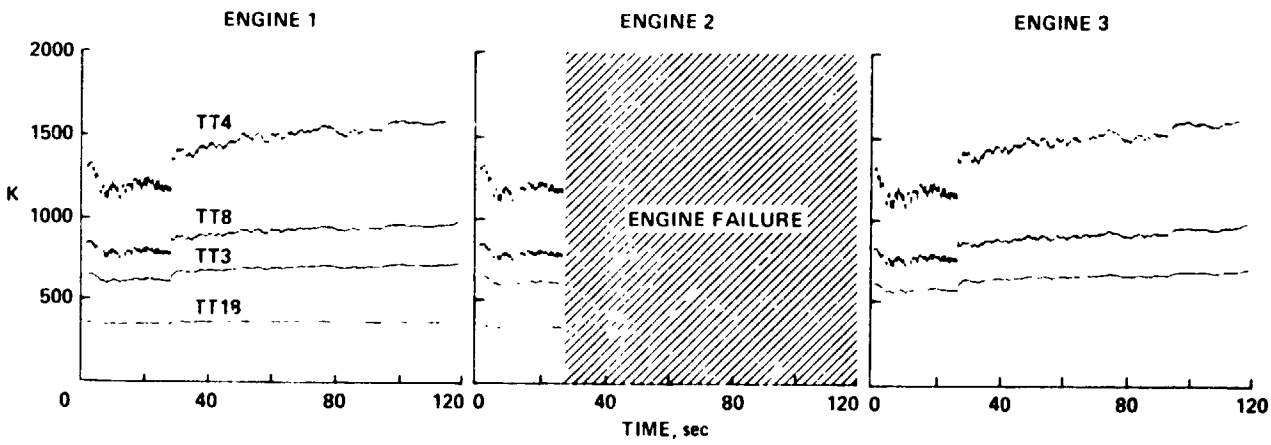

(d) Engine temperatures.

Figure 10.- Continued.

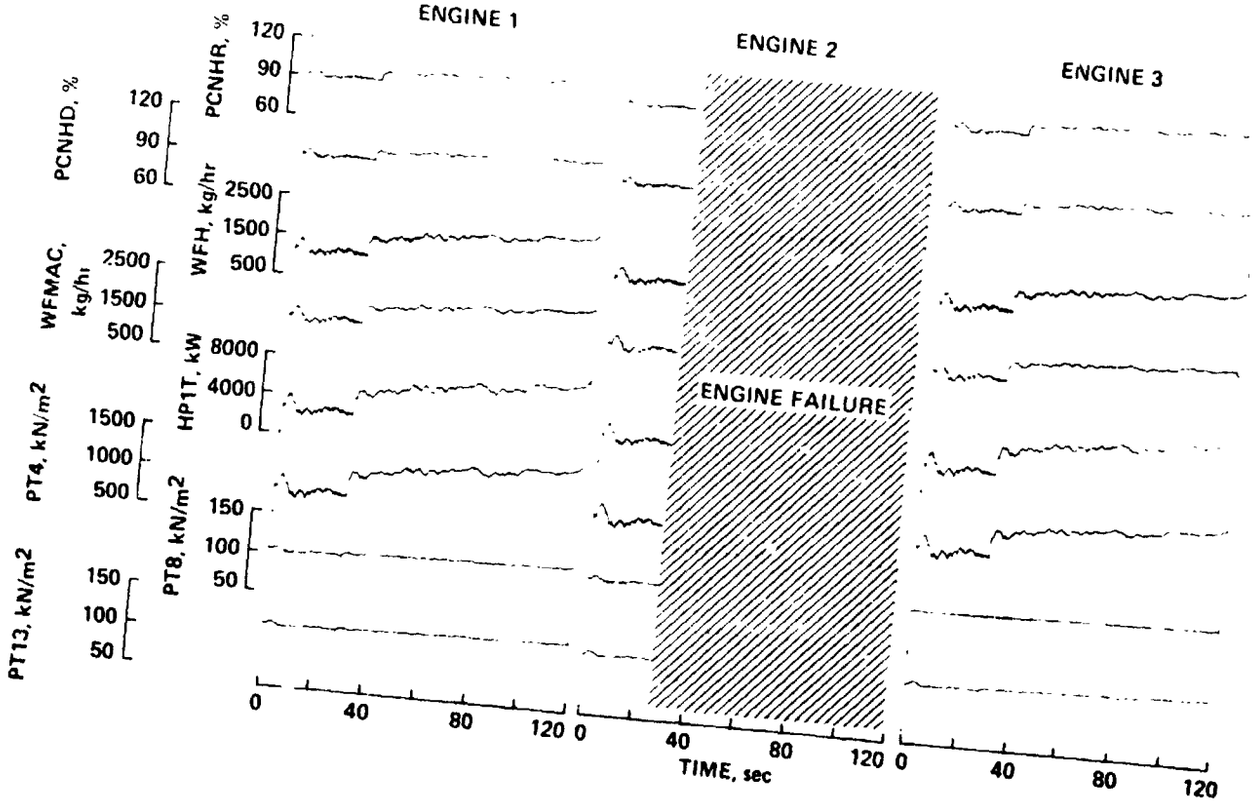

(e) Engine variables.

Figure 10.- Concluded.

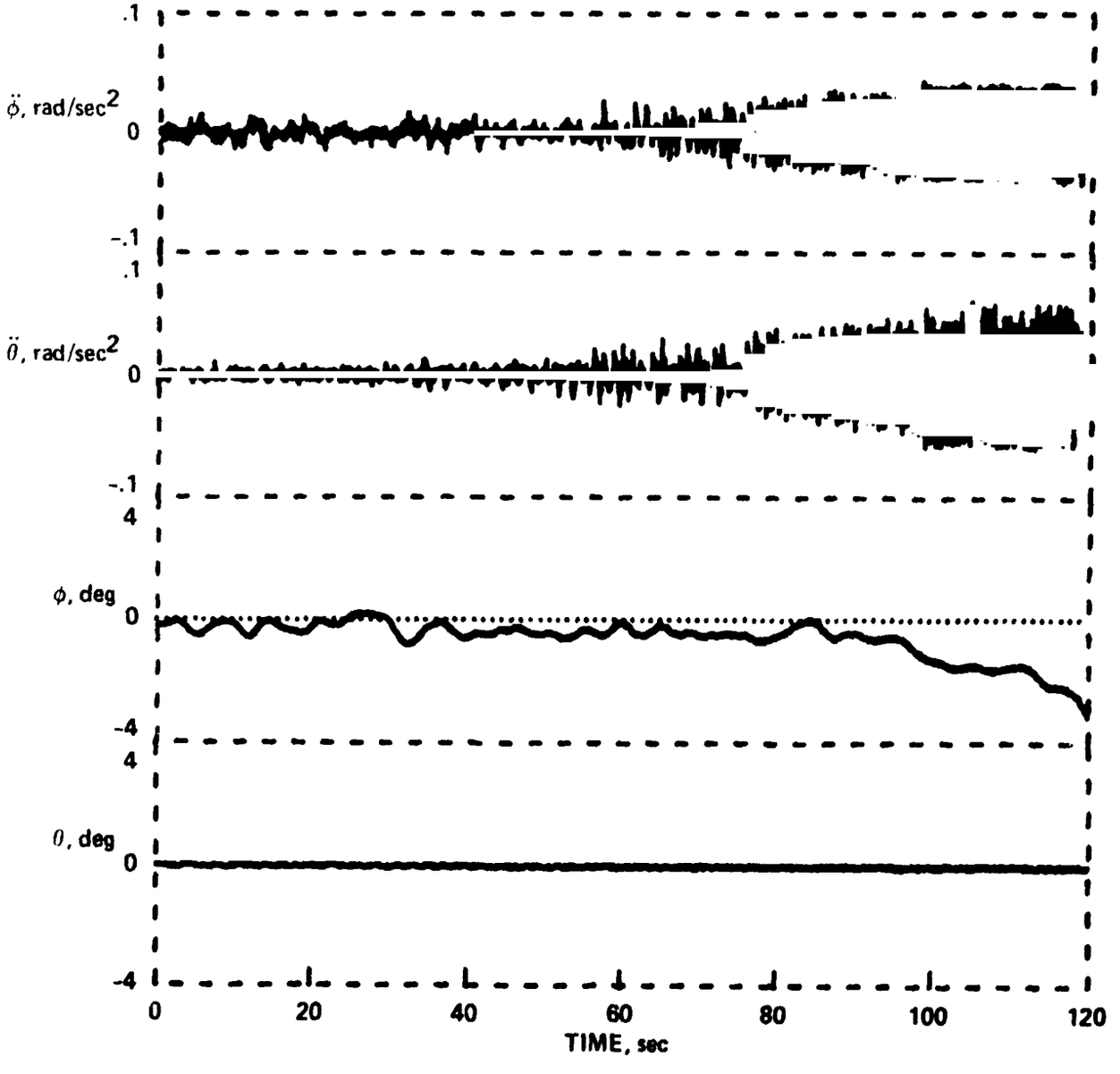

(a) Pitch and roll attitude and acceleration.

Figure 11.- Limit cycle behavior induced by fan blade actuator deadbands. Conditions: 0.5° actuator deadband, 0.25 m/sec rms turbulence.

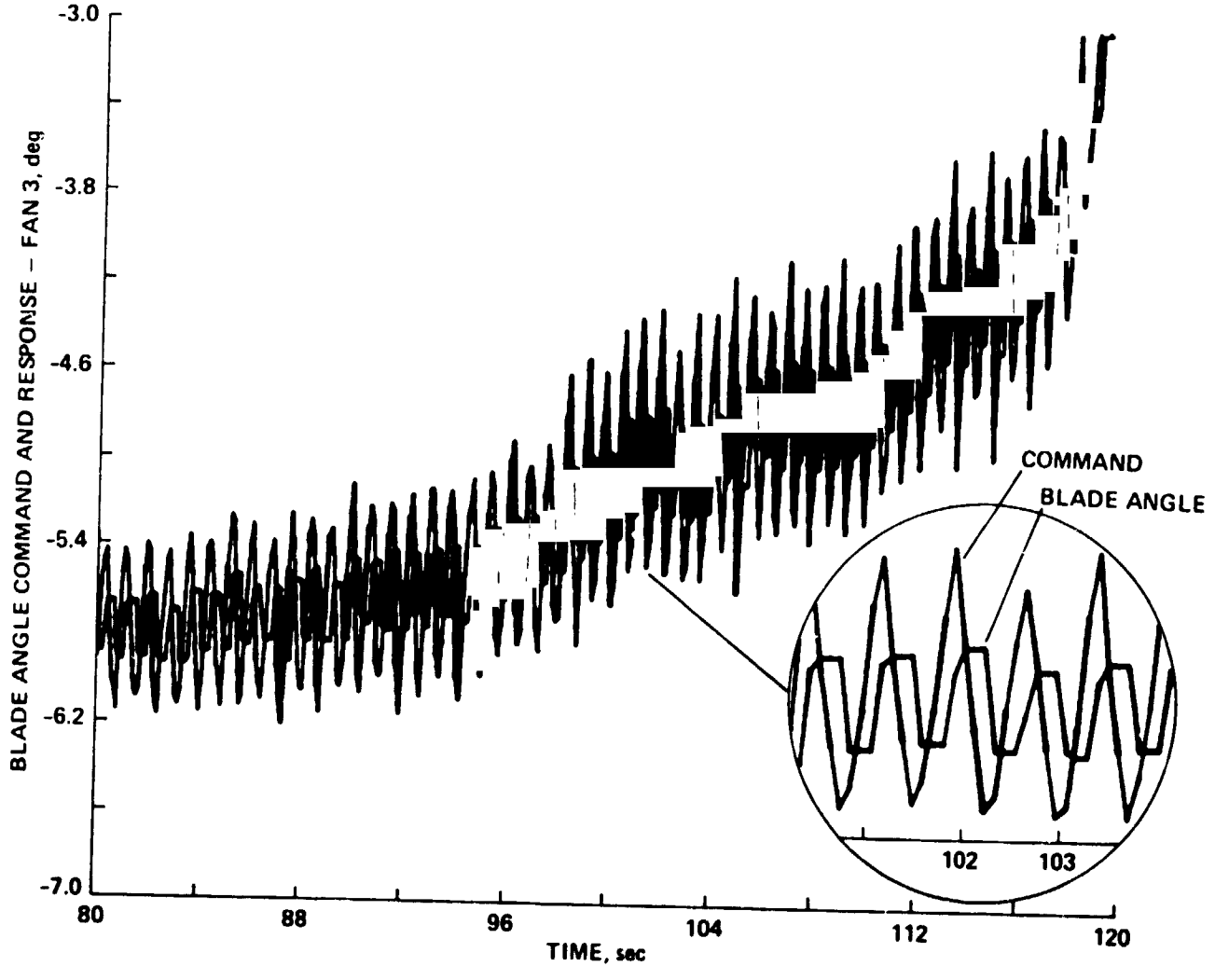

(b) Details of typical fan blade angle command and response.

Figure 11.- Concluded.

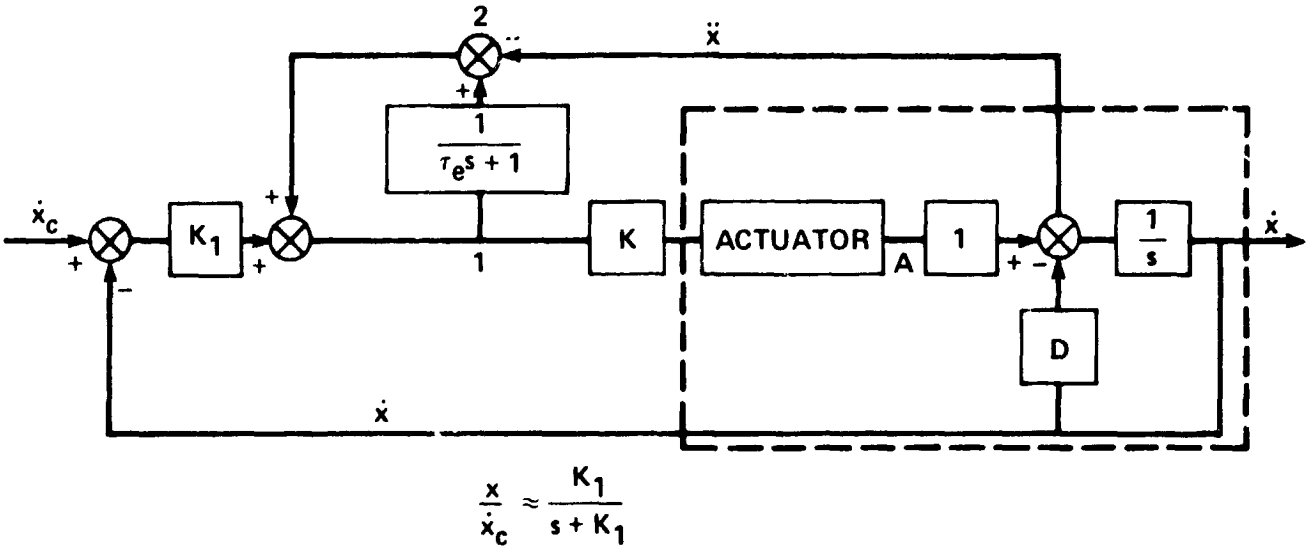

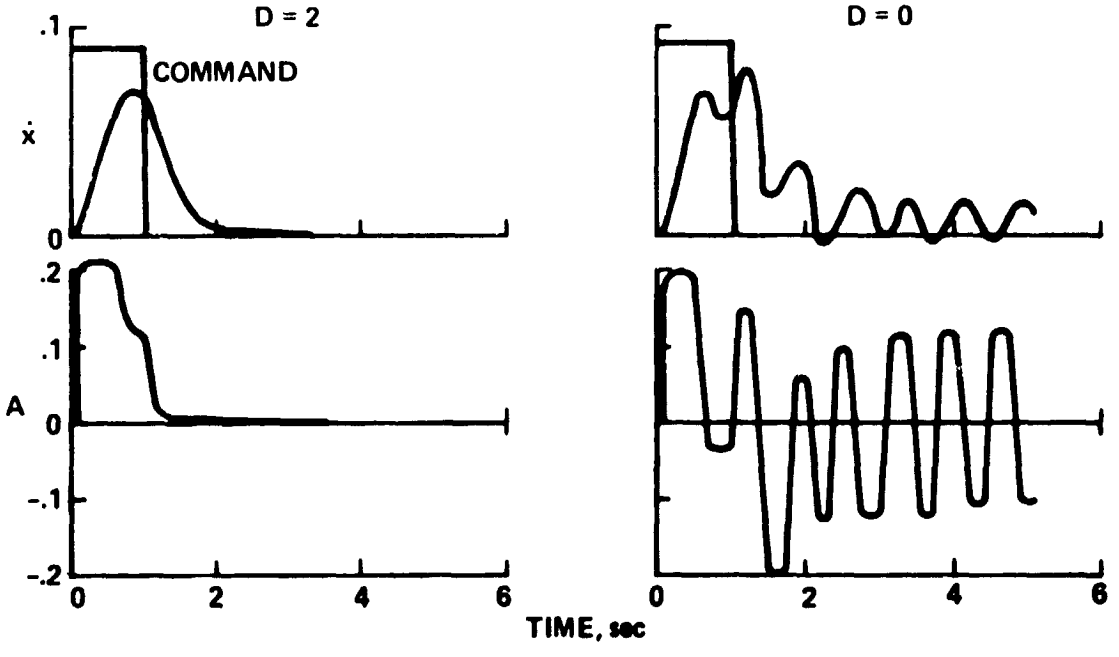

Figure 12.- Effect of a 0.5 actuator deadband on a simple single degree-of-freedom system.

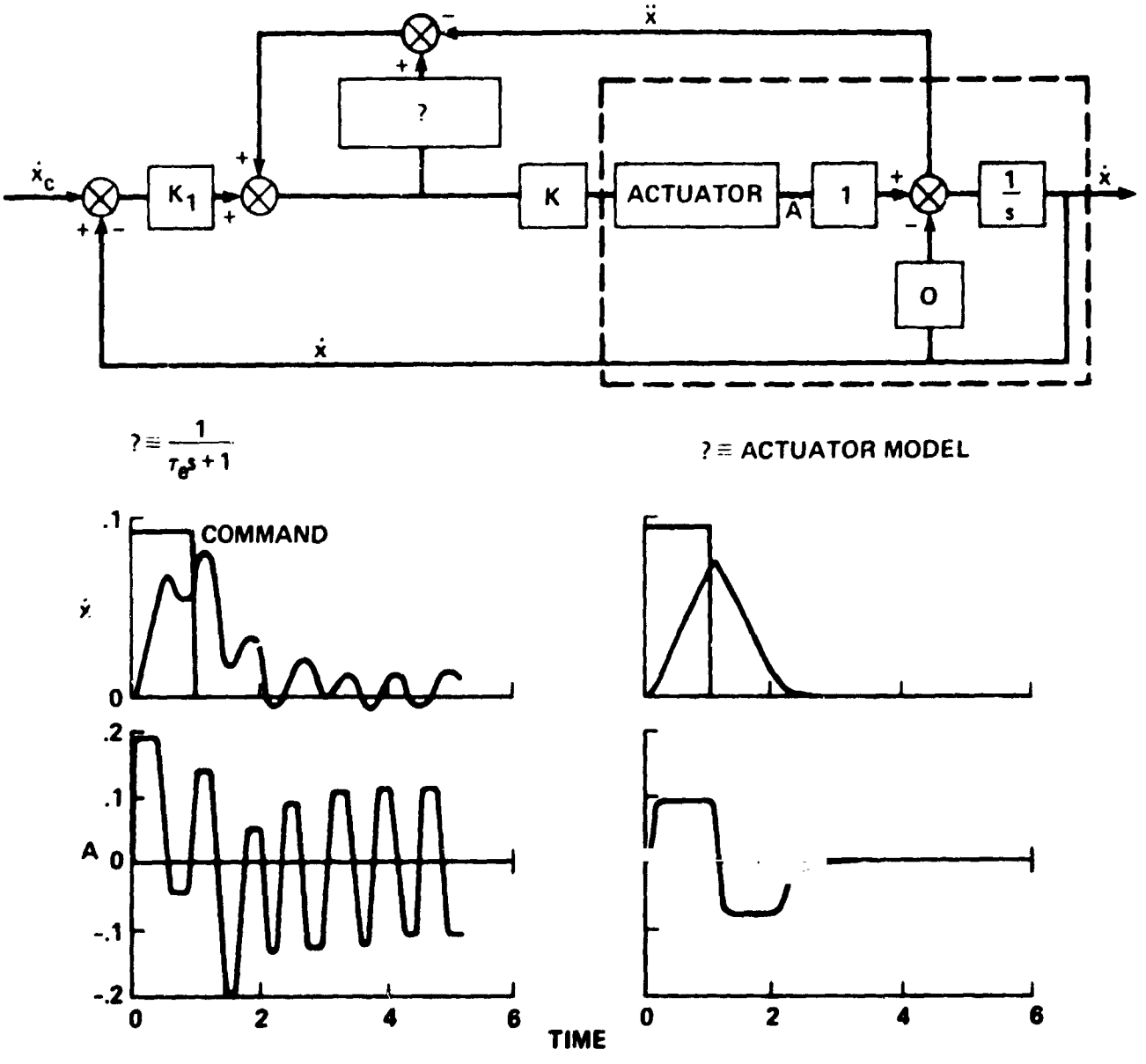

Figure 13.- Deadband compensation technique for simple single degree-of-freedom system.

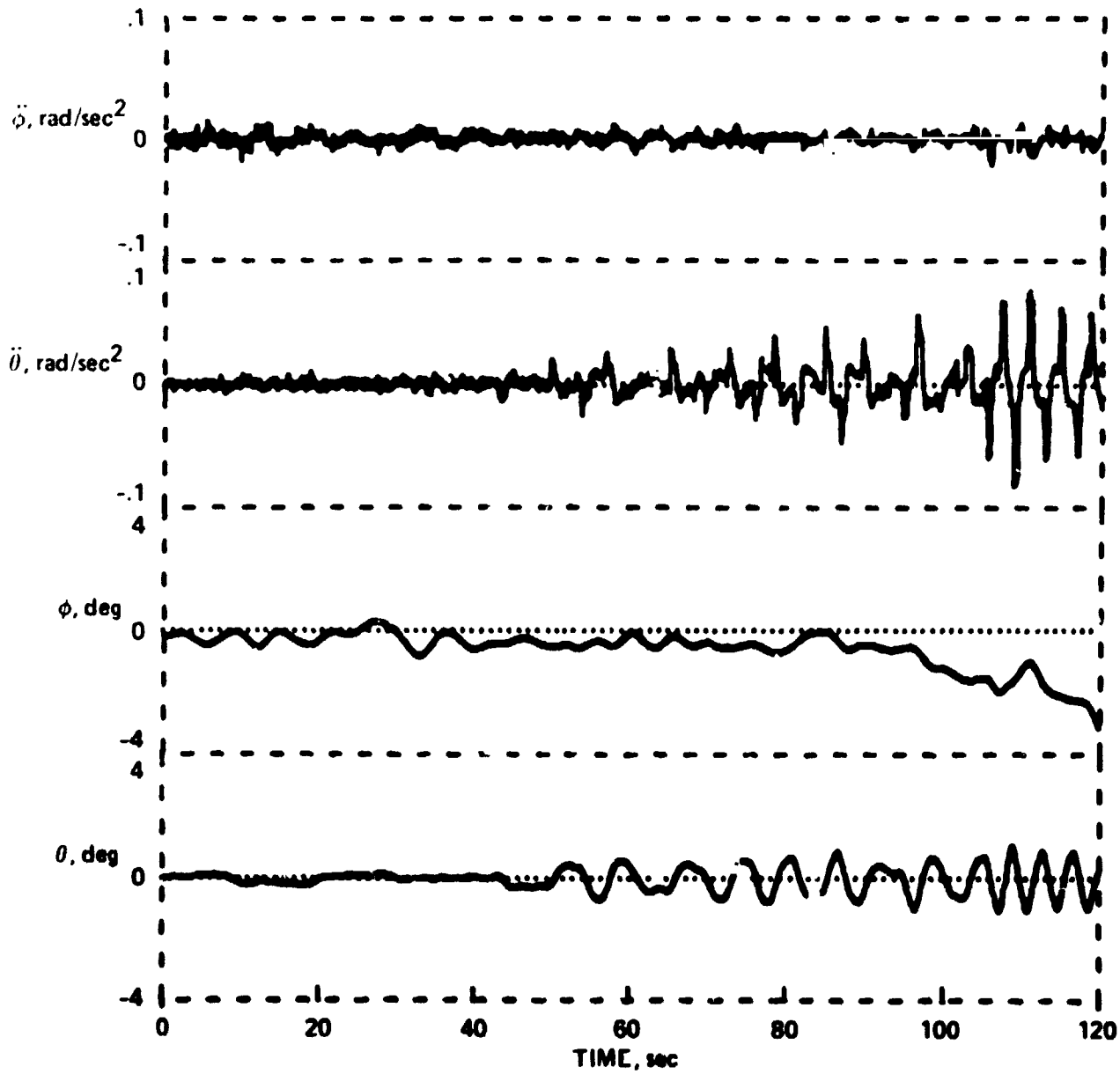

(a) Pitch and roll attitude and acceleration.

Figure 14.- Limit cycle behavior with model-type compensation for actuator deadband. Conditions: 0.5° actuator deadband, 0.25 m/sec rms turbulence.

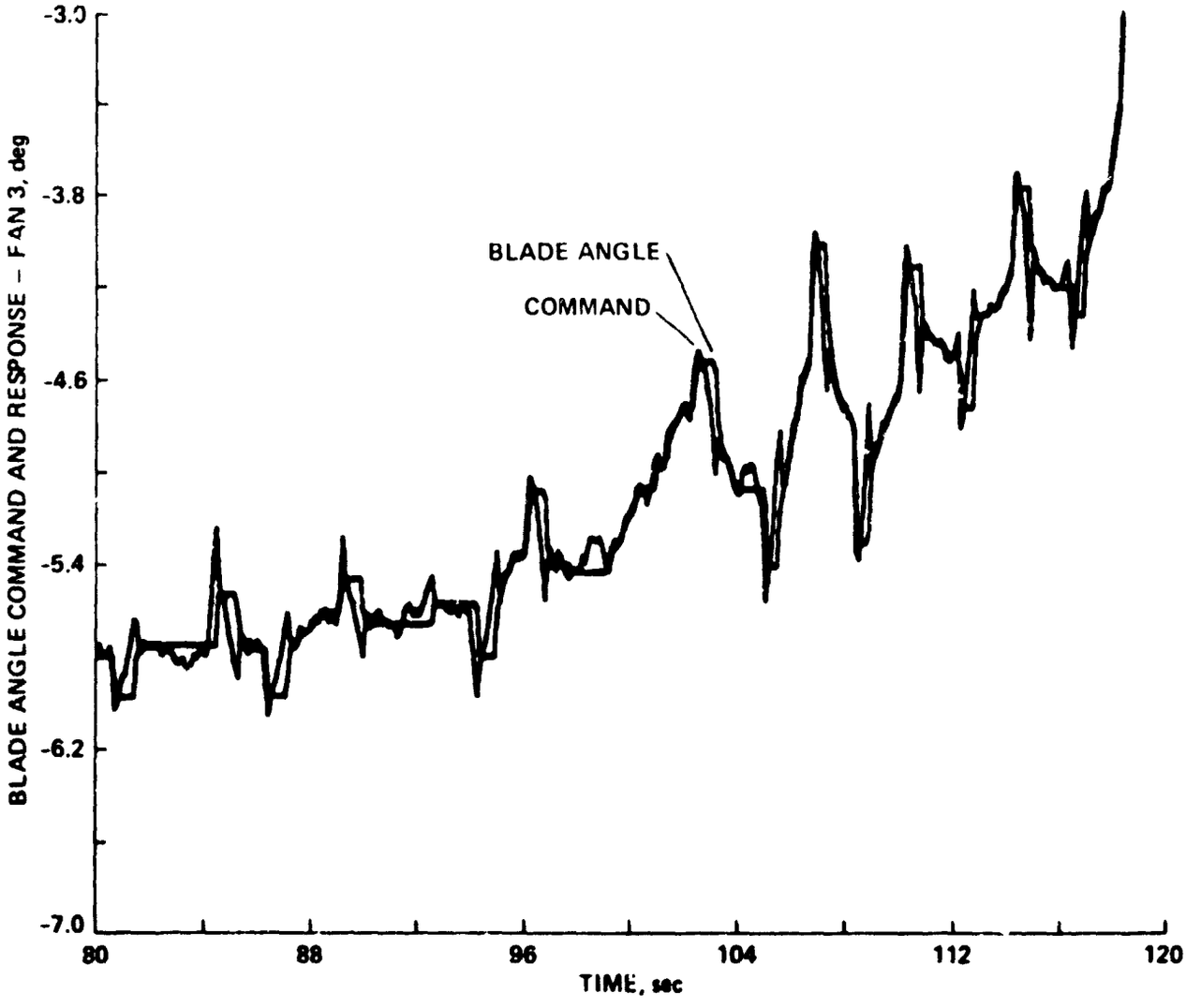

(b) Typical fan blade angle command and response.

Figure 14.- Concluded.

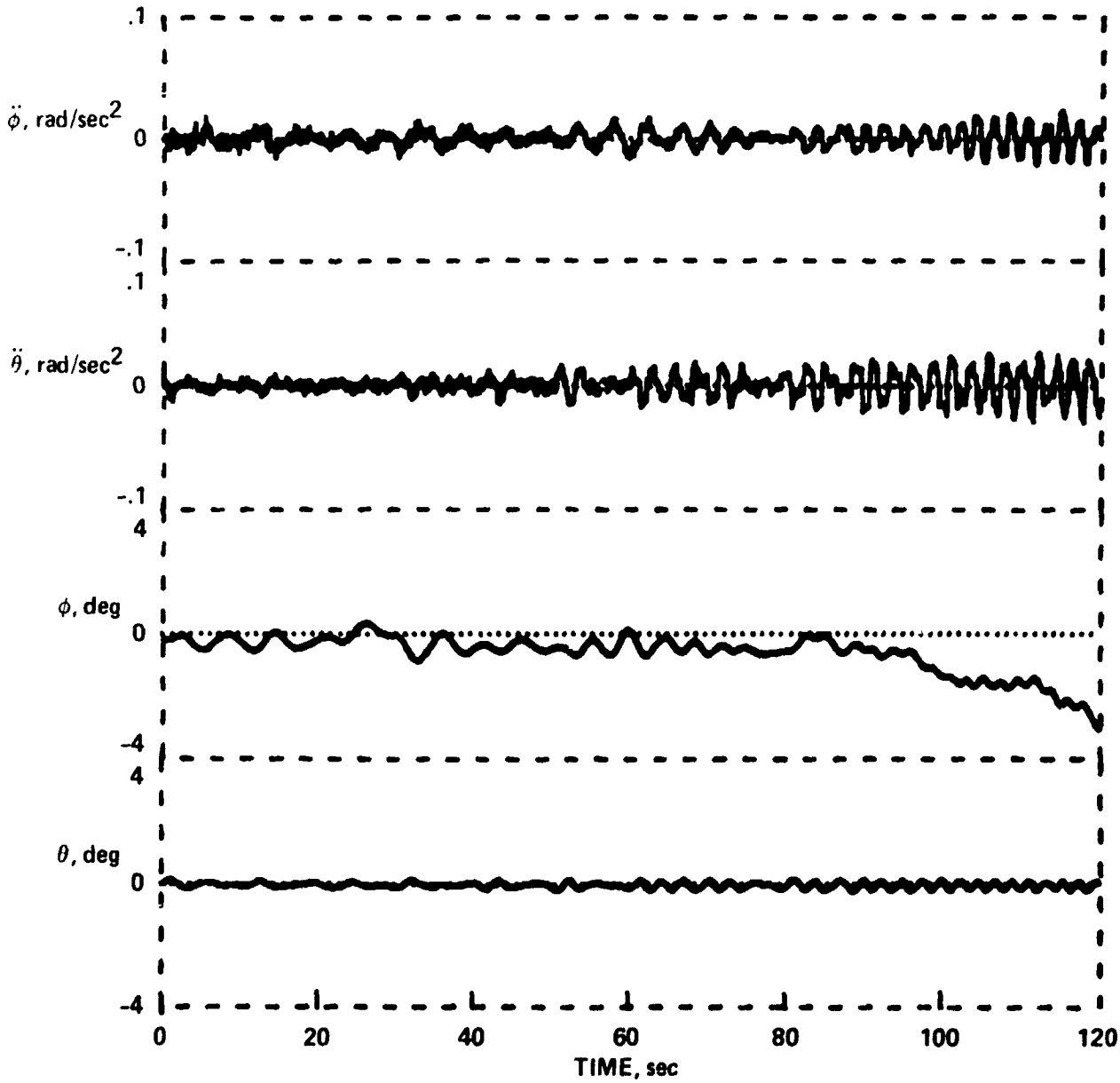

(a) Pitch and roll attitude and acceleration.

Figure 15.- Limit cycle behavior with feedback-type compensation for actuator deadbands. Conditions: 0.5° actuator deadband, 0.25 m/sec rms turbulence.

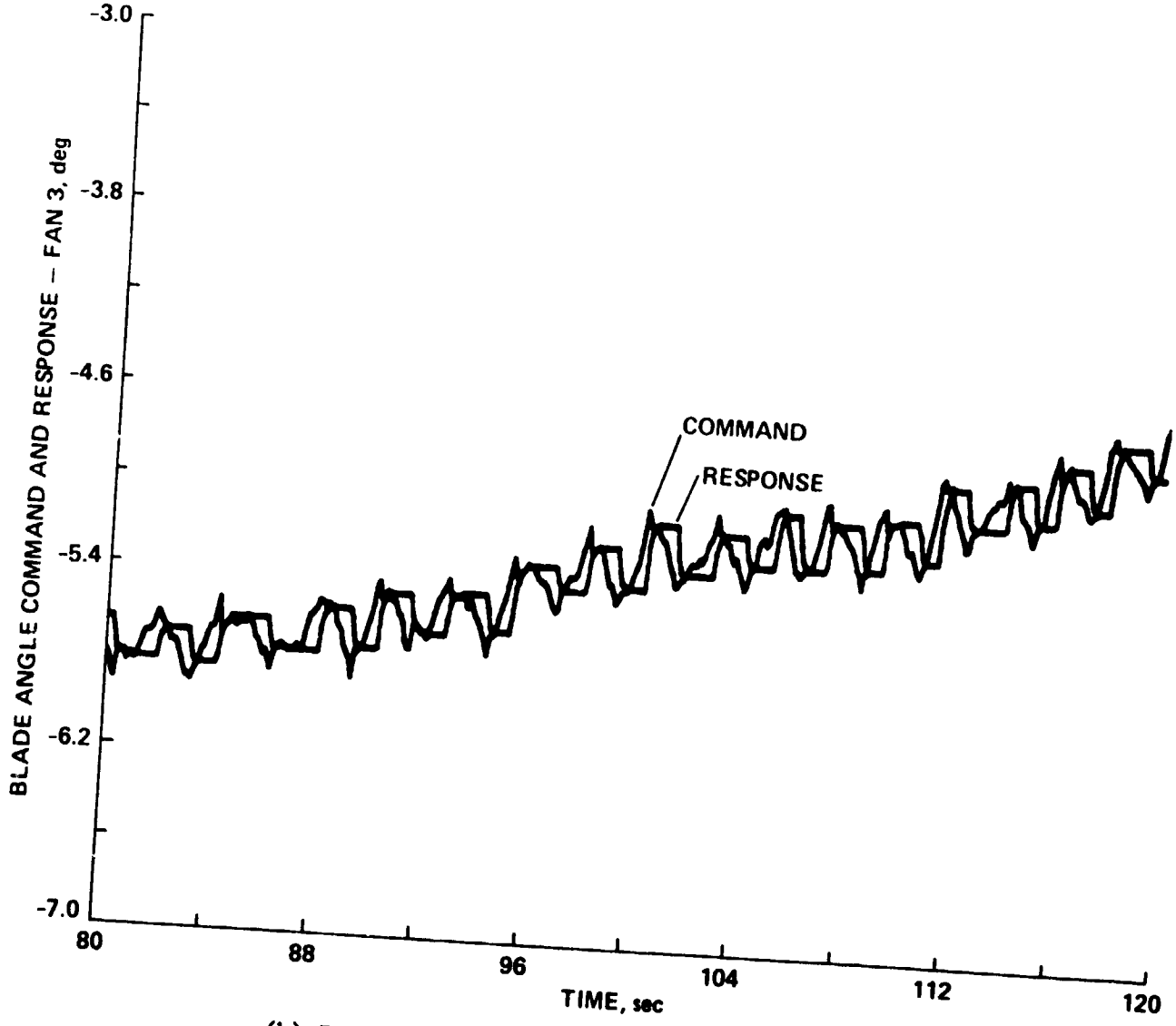

(b) Typical fan blade angle command and response.

Figure 15.- Concluded.

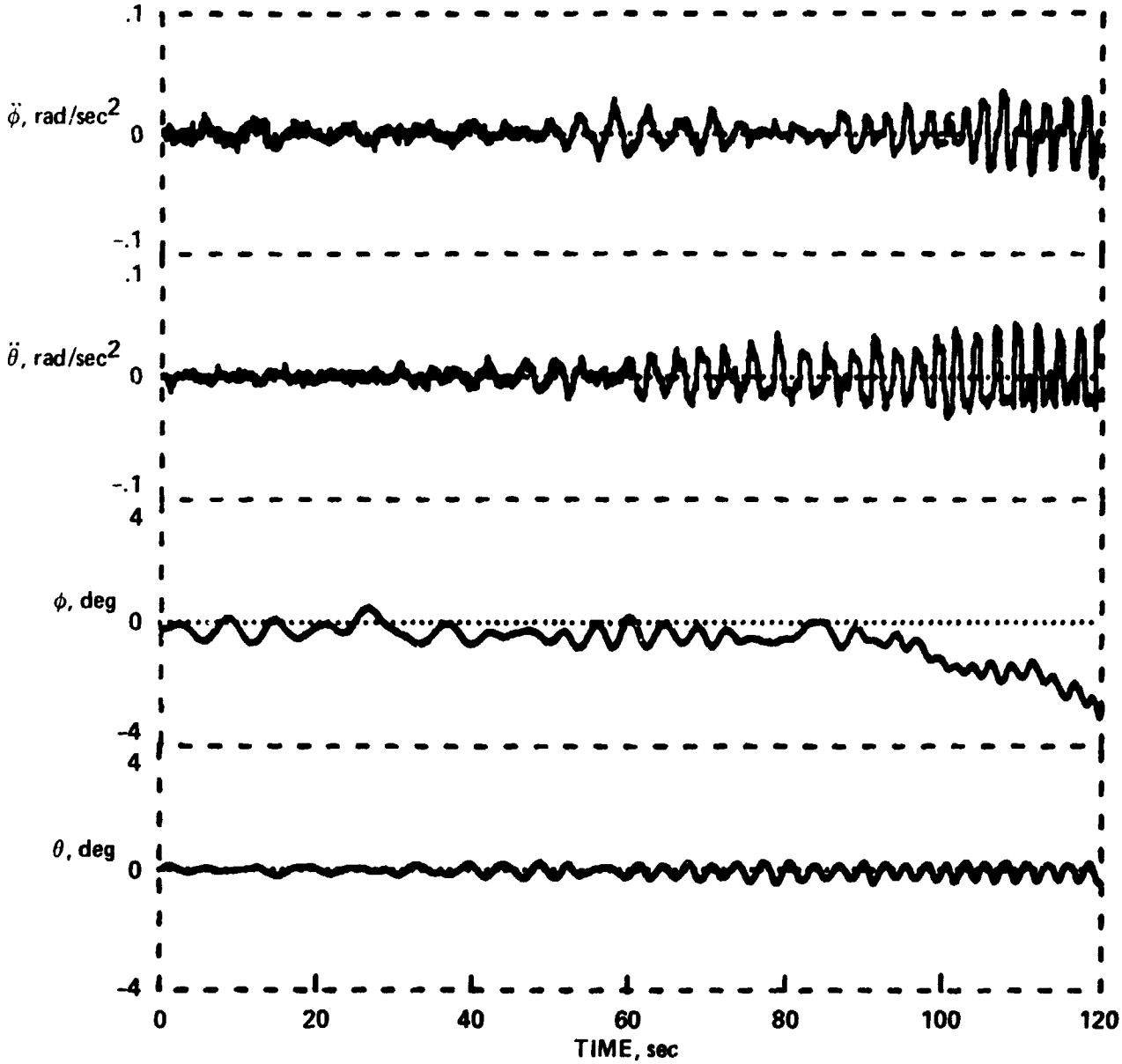

(a) Pitch and roll acceleration.

Figure 16.- Response with actuator time constant for increasing blade angle tripled.

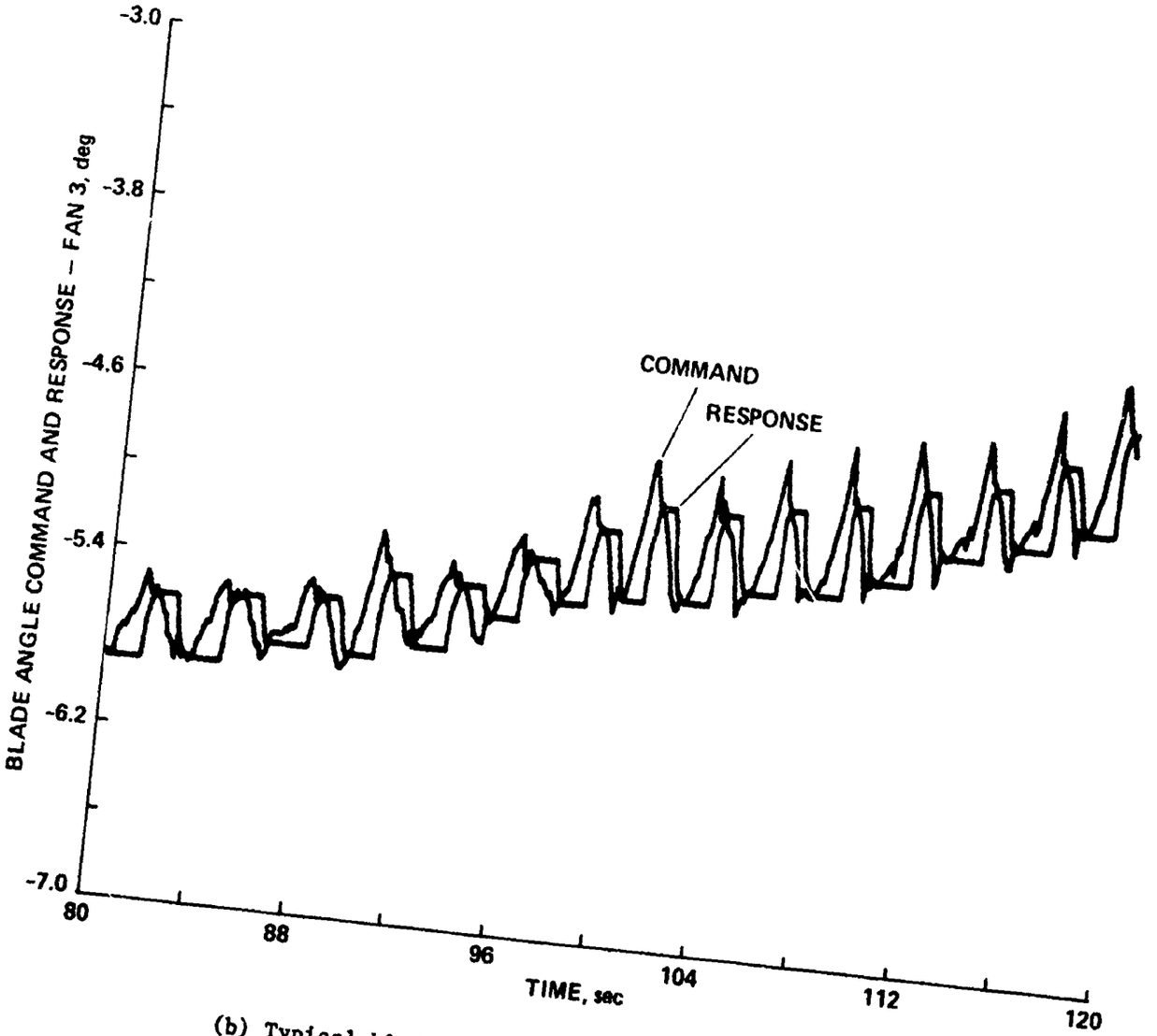

(b) Typical blade angle command and response.

Figure 16.- Concluded.

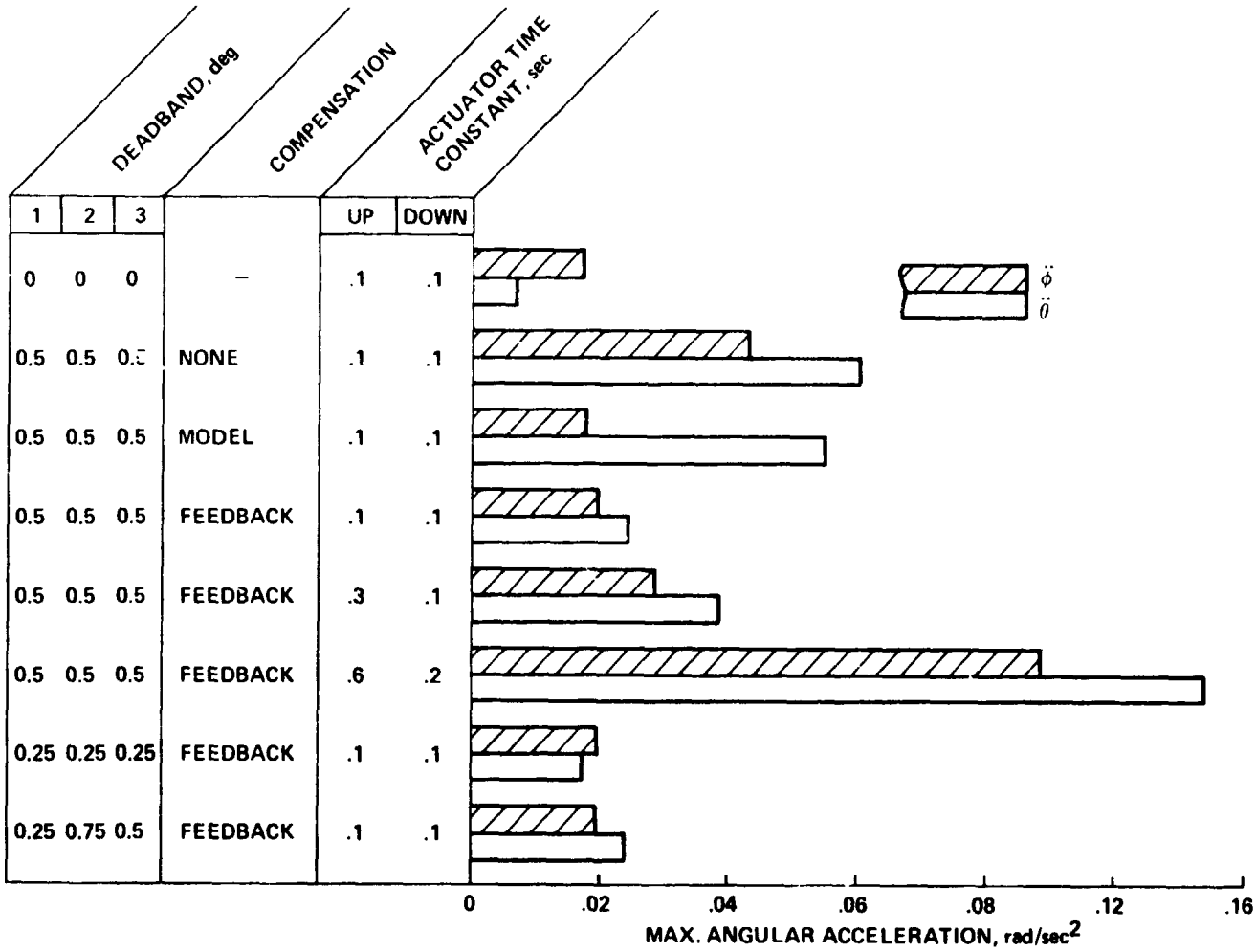

Figure 17.- Effect of deadband, compensation technique, and actuator time constants on maximum angular acceleration in time interval from 5 to 105 sec. RMS turbulence = 0.25 m/sec.

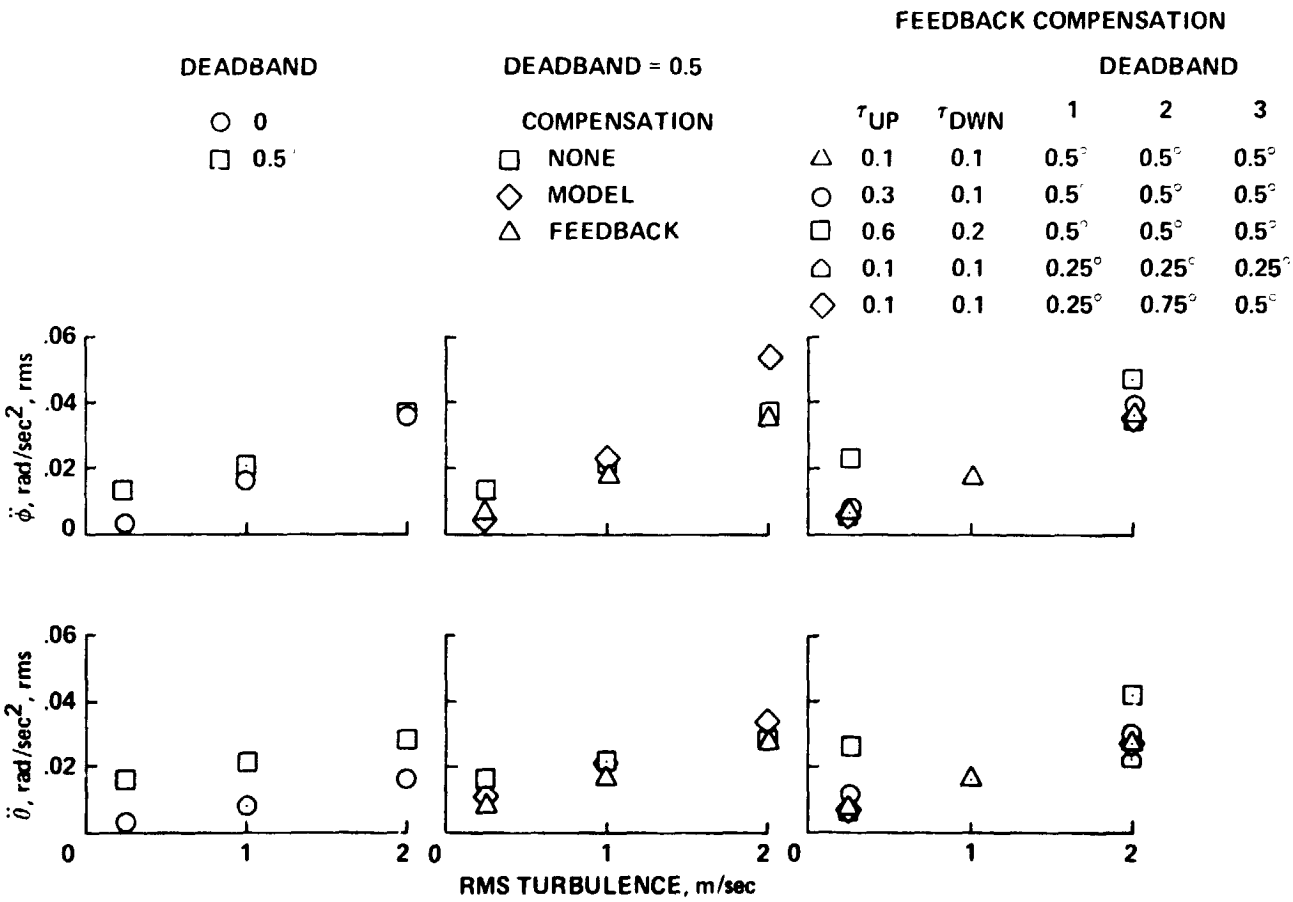

Figure 18.- Effect of turbulence level on rms angular accelerations in time interval from 5 to 105 sec.

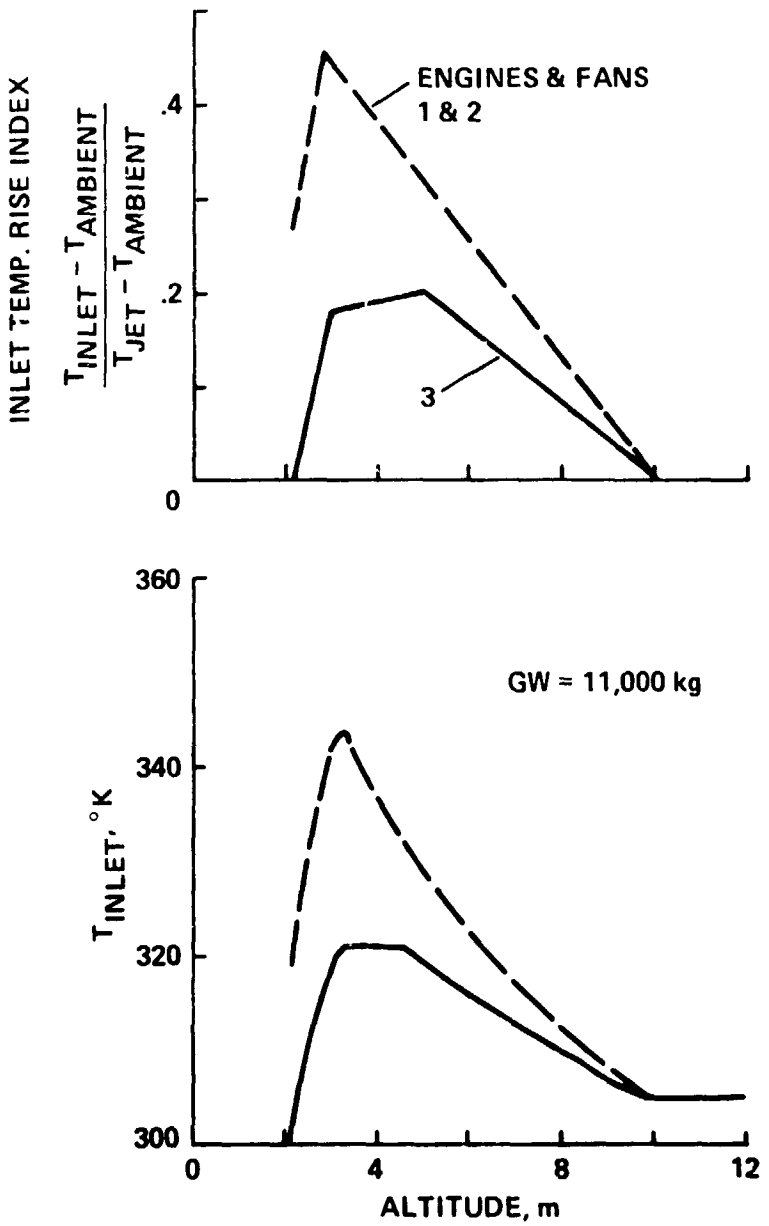

Figure 19.- Inlet temperature rise index and the calculated inlet temperature for a curved decelerating approach.

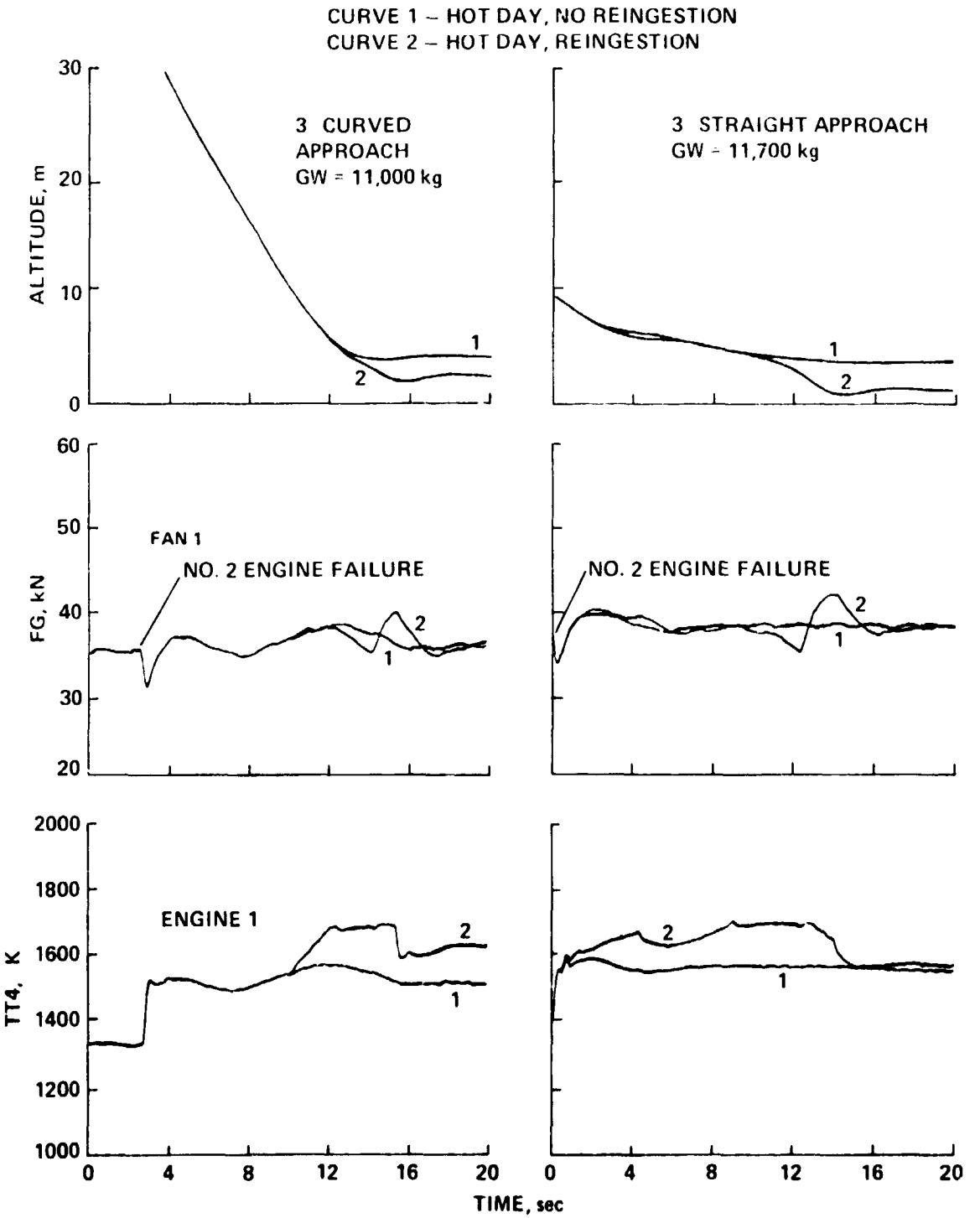

Figure 20.- Effect of temperature rise due to reingestion on flightpath, net fan thrust, and turbine inlet temperature.